

PREDICTION OF DOWNPULL ON HIGH HEAD GATES USING  
COMPUTATIONAL FLUID DYNAMICS

A THESIS SUBMITTED TO  
THE GRADUATE SCHOOL OF NATURAL AND APPLIED SCIENCES  
OF  
MIDDLE EAST TECHNICAL UNIVERSITY

BY

MEHMET AKIŞ UYSAL

IN PARTIAL FULLFILLMENT OF THE REQUIREMENTS  
FOR  
THE DEGREE OF MASTER OF SCIENCE  
IN  
CIVIL ENGINEERING

JANUARY 2014



Approval of the thesis:

**PREDICTION OF DOWNPULL ON HIGH HEAD GATES USING  
COMPUTATIONAL FLUID DYNAMICS**

Submitted by **MEHMET AKIŞ UYSAL** in partial fulfillment of the requirements for the degree of **Master Science in Civil Engineering Department, Middle East Technical University** by,

Prof. Dr. Canan Özgen  
Dean, Graduate School of **Natural and Applied Sciences** \_\_\_\_\_

Prof. Dr. A. Cevdet Yalçın  
Head of Department, **Civil Engineering** \_\_\_\_\_

Assoc. Prof. Dr. Mete Köken  
Supervisor, **Civil Engineering Dept., METU** \_\_\_\_\_

Prof. Dr. İsmail Aydın  
Co-Supervisor, **Civil Engineering Dept., METU** \_\_\_\_\_

**Examining Committee Members**

Prof. Dr. Zafer Bozkuş  
Civil Engineering Dept., METU \_\_\_\_\_

Assoc. Prof. Dr. Mete Köken  
Civil Engineering Dept., METU \_\_\_\_\_

Prof. Dr. İsmail Aydın  
Civil Engineering Dept., METU \_\_\_\_\_

Assoc. Prof. Dr. Şahnaz Tiğrek  
Civil Engineering Dept., METU \_\_\_\_\_

Assoc. Prof. Dr. Funda Kurtuluş  
Aerospace Engineering Dept., METU \_\_\_\_\_

**Date:** 29 January 2014

**I hereby declare that all information in this document has been obtained and presented in accordance with academic rules and ethical conduct. I also declare that, as required by these rules and conduct, I have fully cited and referenced all material and results that are not original to this work.**

Name, Last name : Mehmet Akış UYSAL

Signature :

## **ABSTRACT**

### **PREDICTION OF DOWNPULL ON HIGH HEAD GATES USING COMPUTATIONAL FLUID DYNAMICS**

Uysal, Mehmet Akış

M.Sc., Department of Civil Engineering

Supervisor: Assoc. Prof. Dr. Mete KÖKEN

Co-Supervisor: Prof. Dr. İsmail AYDIN

January 2014, 78 Pages

For design purposes it is important to predict the downpull forces on the tunnel gates installed in the intake of a hydropower plant. In this study downpull forces on the gates are evaluated for different closure rates and for different gate lip geometries using computational fluid dynamics and the results are compared to an existing experimental study. Commercial ANSYS FLUENT software is used in the calculations. It is found that downpull coefficients obtained from computational study showed good agreement with the values calculated from the existing experimental study.

**Keywords:** Downpull, gate lip, computational fluid dynamics, pressure distribution

## ÖZ

### **HİDROLİK KAPAKLARDAKİ HİDRODİNAMİK YÜKLERİN HESAPLAMALI AKIŞKANLAR DİNAMİĞİ KULLANILARAK BELİRLENMESİ**

Uysal, Mehmet Akış

Yüksek Lisans, İnşaat Mühendisliği Bölümü

Tez Yöneticisi: Doç. Dr. Mete KÖKEN

Ortak Tez Yöneticisi: Prof. Dr. İsmail AYDIN

Ocak 2014, 78 Sayfa

Hidroelektrik santrallerin su alma yapısında bulunan hidrolik kapaklar üzerinde oluşan hidrodinamik yüklerin belirlenmesi kapağın tasarımı için önem teşkil etmektedir. Bu çalışmada, kapaklara etkiyen hidrodinamik yükler farklı kapak açıklıklarında ve farklı kapak dudak geometrileri için hesaplamalı akışkanlar dinamiği kullanılarak incelenmiş ve sonuçlar mevcut bir deneysel çalışma ile karşılaştırılmıştır. Hesaplamalarda ticari ANSYS FLUENT yazılımı kullanılmıştır. Hesaplamalı yöntemden elde edilen aşağı çekme kuvvet katsayılarının mevcut deneysel çalışma sonuçları ile uyum içerisinde olduğu bulunmuştur.

Anahtar Kelimeler: Aşağı çekme kuvveti, kapak dudağı, hesaplamalı akışkanlar dinamiği, basınç dağılımı

## **ACKNOWLEDGEMENTS**

The author would like to express his gratitude to supervisor Assoc. Prof. Dr. A. Mete Köken and co-supervisor Prof. Dr. İsmail Aydın for their guidance, advice, criticism, encouragements and insight throughout the research.

## TABLE OF CONTENTS

ABSTRACT .....	V
ÖZ.....	VI
ACKNOWLEDGEMENTS .....	VII
TABLE OF CONTENTS.....	VIII
LIST OF FIGURES .....	X
LIST OF TABLES .....	XIII
LIST OF SYMBOLS AND ABBREVIATIONS .....	XIV
CHAPTERS	
1. INTRODUCTION .....	1
1.1 Description of the Problem.....	1
1.2 Scope and Aim of the Study .....	3
1.3 Literature Review.....	3
2. BACKGROUND .....	7
2.1 Multipurpose Hydraulic Model .....	7
2.2 Forces on a Hydraulic Gate .....	12
2.3 Downpull Force Coefficient .....	13
2.4 Experimental Results .....	14
2.4.1 Pressure Distributions on the Gate Lip .....	14
2.4.2 Lip Downpull Coefficient—Reynolds Number Relationship.....	19
2.4.3 Lip Downpull Coefficient as a Function of the Gate Opening and the Lip Angle.....	22
3. COMPUTATIONAL MODEL .....	25
3.1 Mesh Generation with GAMBIT .....	25
3.1.1 Forming the Geometry .....	25

3.1.2	Forming the Grid.....	28
3.1.3	Clustering .....	29
3.1.4	Near Wall Mesh.....	31
3.1.5	Mesh Size .....	32
3.1.6	Boundary Conditions .....	33
3.2	ANSYS FLUENT Setup and Simulations .....	33
3.2.1	Importing the Mesh.....	33
3.2.2	Scaling, Defining the Material and Gravity .....	33
3.2.3	Turbulence Model.....	34
3.2.4	Boundary Conditions .....	35
3.2.5	Residuals .....	36
3.2.6	Simulations .....	37
3.3	Selecting the Domain Size .....	38
3.4	Grid Dependence Study.....	40
3.5	Computational Results.....	41
3.5.1	Processing for Results .....	41
3.5.2	Computational Models .....	42
3.5.3	Pressure Distributions on the Gate Lip .....	45
3.5.4	Lip Downpull Coefficient—Reynolds Number Relationship .....	50
3.6	Comparison of Selected Flow Properties .....	53
3.6.1	Effect of Gate Opening .....	53
3.6.2	Effect of Lip Angle .....	59
3.6.3	Effect of Discharge .....	64
3.7	Lip Downpull Coefficient as a Function of the Gate Opening and the Lip Angle .....	69
3.8	Comparison of Experimental and Computational Values .....	72
4.	CONCLUSION.....	75
	REFERENCES .....	77

## LIST OF FIGURES

### FIGURES

Figure 2.1 Views from hydraulic model (Aydin et al., 2003).....	8
Figure 2.2 Experimental setup (Aydin et al., 2003) .....	9
Figure 2.3 Details of gate region (Aydin et al., 2003).....	10
Figure 2.4 Gate lip details (Aydin et al., 2003).....	11
Figure 2.5 Pressure distribution on gate lip, Lip A ( $\theta=26.5^\circ$ ). (Aydin et al., 2003) .....	15
Figure 2.6 Pressure distribution on gate lip, Lip B ( $\theta=36.7^\circ$ ). (Aydin et al., 2003) .....	16
Figure 2.7 Pressure distribution on gate lip, Lip C ( $\theta=44.7^\circ$ ). (Aydin et al., 2003) .....	17
Figure 2.8 Pressure distribution on gate lip, Lip D ( $\theta=51.6^\circ$ ). (Aydin et al., 2003) .....	18
Figure 2.9 Downpull coefficient—Reynolds number relationship, $y=0.1$ (Aydin et al., 2003).....	19
Figure 2.10 Downpull coefficient—Reynolds number relationship, $y=0.2$ (Aydin et al., 2003).....	20
Figure 2.11 Downpull coefficient—Reynolds number relationship, $y=0.4$ (Aydin et al., 2003).....	20
Figure 2.12 Downpull coefficient—Reynolds number relationship, $y=0.6$ (Aydin et al., 2003).....	21
Figure 2.13 Downpull coefficient—Reynolds number relationship, $y=0.8$ (Aydin et al., 2003).....	21
Figure 2.14 Downpull coefficient as a function of gate opening and gate lip angle (Aydin et al., 2003) .....	23
Figure 3.1 Geometry formed by GAMBIT .....	27
Figure 3.2 Block based modelling.....	28
Figure 3.3 Mesh refinement .....	30

Figure 3.4 Mesh around the gate .....	31
Figure 3.5 Mesh around gate and parts of upstream and downstream .....	31
Figure 3.6 Near-wall mesh .....	32
Figure 3.7 Residuals.....	38
Figure 3.8 Maximum system discharge (Aydin et al., 2003) .....	43
Figure 3.9 Pressure distribution on gate lip, Lip A ( $\theta=26.5^\circ$ ). (Computational) .....	46
Figure 3.10 Pressure distribution on gate lip, Lip B ( $\theta=36.7^\circ$ ). (Computational).....	47
Figure 3.11 Pressure distribution on gate lip, Lip C ( $\theta=44.7^\circ$ ). (Computational).....	48
Figure 3.12 Pressure distribution on gate lip, Lip D ( $\theta=51.6^\circ$ ). (Computational) .....	49
Figure 3.13 Downpull coefficient—Reynolds number relationship, $y=0.1$ (Computational).....	50
Figure 3.14 Downpull coefficient—Reynolds number relationship, $y=0.2$ (Computational).....	51
Figure 3.15 Downpull coefficient—Reynolds number relationship, $y=0.4$ (Computational).....	51
Figure 3.16 Downpull coefficient—Reynolds number relationship, $y=0.6$ (Computational).....	52
Figure 3.17 Downpull coefficient—Reynolds number relationship, $y=0.8$ (Computational).....	52
Figure 3.18 Velocity magnitude distribution for (A) $\theta=26.5^\circ$ , $y=0.1$ , $Q=0.0295 \text{ m}^3/\text{s}$ , (B) $\theta=26.5^\circ$ , $y=0.5$ , $Q=0.1107 \text{ m}^3/\text{s}$ , (C) $\theta=26.5^\circ$ , $y=0.9$ , $Q=0.1216 \text{ m}^3/\text{s}$ .....	55
Figure 3.19 Velocity profiles under the gate section for $y=0.1$ , $y=0.5$ and $y=0.9$ .....	56
Figure 3.20 Streamlines for (A) $\theta=26.5^\circ$ , $y=0.1$ , $Q=0.0295 \text{ m}^3/\text{s}$ , (B) $\theta=26.5^\circ$ , $y=0.5$ , $Q=0.1107 \text{ m}^3/\text{s}$ , (C) $\theta=26.5^\circ$ , $y=0.9$ , $Q=0.1216 \text{ m}^3/\text{s}$ .....	57
Figure 3.21 Turbulent Kinetic Energy for (A) $\theta=26.5^\circ$ , $y=0.1$ , $Q=0.0295 \text{ m}^3/\text{s}$ , (B) $\theta=26.5^\circ$ , $y=0.5$ , $Q=0.1107 \text{ m}^3/\text{s}$ , (C) $\theta=26.5^\circ$ , $y=0.9$ , $Q=0.1216 \text{ m}^3/\text{s}$ .....	58
Figure 3.22 Velocity magnitude distribution for (A) $\theta=26.5^\circ$ , $y=0.4$ , $Q=0.0947 \text{ m}^3/\text{s}$ , (B) $\theta=36.7^\circ$ , $y=0.4$ , $Q=0.0997 \text{ m}^3/\text{s}$ , (C) $\theta=44.7^\circ$ , $y=0.4$ , $Q=0.0955 \text{ m}^3/\text{s}$ , (D) $\theta=51.6^\circ$ , $y=0.4$ , $Q=0.0953 \text{ m}^3/\text{s}$ .....	60

Figure 3.23 Velocity profiles under the gate section for  $\theta=26.5^\circ$ ,  $\theta=36.7^\circ$ ,  $\theta=44.7^\circ$  and  $\theta=51.6^\circ$ ..... 61

Figure 3.24 Streamlines for (A)  $\theta=26.5^\circ$ ,  $y=0.4$ ,  $Q=0.0947 \text{ m}^3/\text{s}$ , (B)  $\theta=36.7^\circ$ ,  $y=0.4$ ,  $Q=0.0997 \text{ m}^3/\text{s}$ , (C)  $\theta=44.7^\circ$ ,  $y=0.4$ ,  $Q=0.0955 \text{ m}^3/\text{s}$ , (D)  $\theta=51.6^\circ$ ,  $y=0.4$ ,  $Q=0.0953 \text{ m}^3/\text{s}$  ..... 62

Figure 3.25 Turbulent Kinetic Energy for (A)  $\theta=26.5^\circ$ ,  $y=0.4$ ,  $Q=0.0947 \text{ m}^3/\text{s}$ , (B)  $\theta=36.7^\circ$ ,  $y=0.4$ ,  $Q=0.0997 \text{ m}^3/\text{s}$ , (C)  $\theta=44.7^\circ$ ,  $y=0.4$ ,  $Q=0.0955 \text{ m}^3/\text{s}$ , (D)  $\theta=51.6^\circ$ ,  $y=0.4$ ,  $Q=0.0953 \text{ m}^3/\text{s}$ ..... 63

Figure 3.26 Velocity magnitude distribution for (A)  $\theta=51.6^\circ$ ,  $y=0.2$ ,  $Q=0.0075 \text{ m}^3/\text{s}$ , (B)  $\theta=51.6^\circ$ ,  $y=0.2$ ,  $Q=0.0343 \text{ m}^3/\text{s}$ , (C)  $\theta=51.6^\circ$ ,  $y=0.2$ ,  $Q=0.0487 \text{ m}^3/\text{s}$  ..... 65

Figure 3.27 Velocity profiles under the gate section for  $Q=0.0075 \text{ m}^3/\text{s}$ ,  $Q=0.0343 \text{ m}^3/\text{s}$  and  $Q=0.0487 \text{ m}^3/\text{s}$  ..... 66

Figure 3.28 Streamlines for (A)  $\theta=51.6^\circ$ ,  $y=0.2$ ,  $Q=0.0075 \text{ m}^3/\text{s}$ , (B)  $\theta=51.6^\circ$ ,  $y=0.2$ ,  $Q=0.0343 \text{ m}^3/\text{s}$ , (C)  $\theta=51.6^\circ$ ,  $y=0.2$ ,  $Q=0.0487 \text{ m}^3/\text{s}$  ..... 67

Figure 3.29 Turbulent Kinetic Energy for (A)  $\theta=51.6^\circ$ ,  $y=0.2$ ,  $Q=0.0075 \text{ m}^3/\text{s}$ , (B)  $\theta=51.6^\circ$ ,  $y=0.2$ ,  $Q=0.0343 \text{ m}^3/\text{s}$ , (C)  $\theta=51.6^\circ$ ,  $y=0.2$ ,  $Q=0.0487 \text{ m}^3/\text{s}$  ..... 68

Figure 3.30 Downpull coefficient as a function of the gate lip angle and the gate opening (Computational) ..... 71

Figure 3.31 Downpull coefficient as a function of the gate lip angle and the gate opening (Computational and experimental comparison) ..... 74

## LIST OF TABLES

### TABLES

Table 2.1 Gate lip angles.....	11
Table 3.1 Material Definition.....	34
Table 3.2 Turbulence Model.....	35
Table 3.3 Wall Roughness Properties.....	36
Table 3.4 System Configurations.....	37
Table 3.5 Variation in $K_L$ for different upstream lengths.....	39
Table 3.6 Variation in $K_L$ for different downstream lengths.....	39
Table 3.7 Grid points and $K_L$ comparison.....	41
Table 3.8 Simulations carried out ( $\theta=26.5^\circ$ and $\theta=36.7^\circ$ ).....	44
Table 3.9 Simulations carried out ( $\theta=44.7^\circ$ and $\theta=51.6^\circ$ ).....	44

## LIST OF SYMBOLS AND ABBREVIATIONS

2D	Two dimensional
3D	Three dimensional
A	Cross sectional area of the gate on horizontal plane
$A_{hL}$	Horizontally projected area of the gate lip
CFD	Computational fluid dynamics
d/s	Downstream
$D_p$	Downpull force on the gate
e	Gate opening
$e_0$	Tunnel height
g	Gravitational acceleration
H	Operating head on the gate bottom
$H_1$	Reservoir water level
$h_2$	Water level in the gate
$h_2^*$	Piezometric head just upstream from the gate
$h_3$	Water level in gate chamber
$H_4$	Tail water level
$\bar{h}_1$	Average piezometric head acting on the gate lip
$h_p$	Piezometric head of the gate lip
$K_L$	Downpull force coefficient
p	Pressure
Q	Discharge
r	Radius of the curvature of the gate lip entrance
Re	Reynolds number
$R_g$	Reynolds number under the gate lip cross section

$s$	Distance along inclined surface of the gate lip
TKE	Turbulent kinetic energy
u/s	Upstream
$U_g$	Average velocity under the gate lip cross section
$y$	Dimensionless gate opening ( $e/e_0$ )
$y^+$	Dimensionless wall distance
$\gamma_w$	Specific weight of water
$\theta$	Lip angle



## CHAPTER 1

### INTRODUCTION

#### 1.1 Description of the Problem

Rectangular cross-sectioned vertical leaf gates are commonly used in large cross-sectional conduits, such as penstocks, which is the intake structure that controls water flow and delivers water to hydraulic turbines. These gates are used for discharge control and emergency closure operations. Vertical leaf gates are widely favored because they are easily constructed, installed and easy on maintenance, comparing to the other types of gates.

Because of being operated mostly under high heads, these vertical gates are under serious forces while operating, which can be described as hydrodynamic loading, uplift or downpull. The high speed water passing under the gate may lead to strong vibration problems on the gate and on the hoisting mechanisms. These forces depend on several parameters, including variables such as pipe and gate geometry.

It is a known fact that the bottom gate geometry plays an important role while predicting these forces. The bottom of the gate, also known as the “gate lip” has a great influence on several factors, such as cavitation damage on the gate, gate vibrations, downpull and uplift forces on the gate and the discharge coefficient.

Many studies have been carried out in order to eliminate cavitation damage and vibrations, minimize downpull or uplift and maximize the discharge coefficient. Among these mentioned factors, downpull is considered to be of great importance.

Downpull forces on the gate occur by a reduced pressure while a fluid flows under the gate. Since these forces act in the closing direction of the gate, the main concern arises for the hoisting equipment of the gate. The hoist mechanism need to withstand the weight of the gate and the downpull. In other words, hydrodynamic downpull determines the hoist capacity of the gate, since the hoisting equipment plus frictional forces need to resist downpull forces and weight of the gate. Occasionally, an uplift may occur if there is a negative downpull, which may result in failure of gate closure if the gate is not heavy enough, thus not sufficient to withstand this uplift force.

In order to determine the downpull, a pressure distribution profile on the gate has to be measured or predicted. Studies show that the downpull on the gate is affected by both the geometry of the gate and the rate of flow passing under the gate.

An easy to use lip downpull coefficient was introduced as a function of the lip angle and the gate opening (Aydin et al., 2006). This dimensionless coefficient was calculated for different gate lips and openings. Data coming from these experiments were summarized as a function of lip angle and the gate opening and this function was intended to be used in the prediction of downpull forces.

For investigating the effects of downpull, small scale model experiments have been done for a long period of time. This approach generally results in high costs, measurement difficulties, scaling problems and depends on the availability of equipment. Again, due to the complexity and nonlinearity of the governing equations, the analytical approach is also not considered as an advantageous approach compared to the experimental models.

On the other hand, numerical methods are considered to be notable approaches in the recent years. As a result of advancements in computational power, computational fluid dynamics (CFD) became more of a great importance and these advancements led a great progression on this approach. As a result, numerical simulations became a major approach, especially since the development of capable software.

## **1.2 Scope and Aim of the Study**

This study is an attempt to validate results from experimental studies, carried out by Aydin et al. (2002, 2003, 2006), which experiments were conducted in the Hydromechanics Laboratory of Civil Engineering Department at METU.

The aim of the thesis is to examine pressure distribution on the gate lips for different lip angles and gate openings with variable discharges using computational fluid dynamics, with the aid of commercial GAMBIT and ANSYS FLUENT software and to compare the results coming from the experimental setup of the system.

A dimensionless downpull force coefficient will be obtained from computational calculations and will be compared to the downpull force coefficient coming from the original experiments. Previous experimental study on this subject showing all steps will be summarized for better understanding the concept.

This thesis is intended to demonstrate the potential use of computational fluid dynamics by validating results with the experimental data.

## **1.3 Literature Review**

Hydrodynamic loadings on hydraulic gates were investigated on hydraulic models. Variables measured from hydraulic models were represented by graphics using dimensionless parameters and are used to predict hydrodynamic loadings (Naudascher 1986, 1991). For this purpose, empirical formulas were also offered (Naudascher 1991). A one-dimensional analysis of the discharge passing under a gate and downpull acting on the same gate was presented by Naudascher et al. (1964, 1986).

It is claimed that geometrical characteristics of the gates such as operating head, gate opening and bottom gate geometry, have a great influence on net downpull on a high head vertical leaf gate (Sagar, 1977). In addition to geometry, boundary layers and turbulence

have effects on the downpull on the gate. Sagar stated that gate hoist capacity must be determined precisely in order to ensure a risk-free closure of the gates.

A numerical analysis for calculating viscous flows controlled by a vertical lift gate and hydrodynamic forces acting on the gate was developed by Amorim and Andrade (1999). The numerical solution is obtained from the incompressible Navier-Stokes equations and turbulence effects are simulated by a  $k-\varepsilon$  turbulence model. After completing simulations with the numerical model, Amorim and Andrade compared results with available experimental data at various opening positions.

Aydin (2002) investigated pressure drop and consecutive air demand behind high head gates during emergency closure by physical and mathematical models. Aydin formed a mathematical model for the unsteady flow due to closing gate by applying the integral continuity and energy equations on control volumes upstream and downstream of the gate.

Hydrodynamic loadings acting on closing high head leaf gates, are studied experimentally on hydraulic models and a mathematical model is developed and published as a part of the research project titled as “Hydrodynamic Downpull on Closing Hydraulic Gates” (Aydin et al., 2003).

Experimental work on downpull force on gates installed in the intake structures of hydroelectric power plants including lip pressure distribution measurements and direct weighing of downpull are presented by Aydin et al. (2006).

Akoz et al. (2009) have conducted laboratory experiments to measure the velocities of a 2D open channel flow under a sluice gate and carried out simulations using computational fluid dynamics. Akoz had used different mesh sizes to investigate the effects of the mesh size and compared  $k-\varepsilon$  and  $k-\omega$  turbulence models for the same model. Akoz found out that  $k-\varepsilon$  turbulence model has predicted the velocity field more accurate and faster by means of simulation time, than the  $k-\omega$  model.

Dargahi (2010) investigated the discharge characteristics of a bottom outlet with a moving gate by FLOW-3D software. Dargahi used experimental results for an existing scale model and measured pressurized and free-surface flow features. Dargahi found out that the velocity and pressure distributions were predicted by the numerical analysis within a maximum error of 2.6% and 10%, respectively.



## CHAPTER 2

### BACKGROUND

#### 2.1 Multipurpose Hydraulic Model

All experiments summarized in this chapter were conducted by Aydin et al. in 2003, as a part of a research project supported by METU and TÜBİTAK. The results were presented in the report which was published in 2003.

For studying the effects of hydrodynamic downpull on different gate lips and gate openings, a physical model for a typical intake structure was constructed as the multipurpose hydraulic model by Aydin et al. (2003). All experiments were conducted on this model. The general view of the model is shown in Figure 2.1 and the details are shown in Figure 2.2 (not scaled).

Starting from the upstream, system consists of a reservoir, an intake region, 0.30 m x 0.24 m rectangular cross-sectioned gate area, a ventilation shaft, transition from rectangular to circular cross section, circular shaped penstock, a control valve representing a turbine and an open channel which is used for measuring the tail water level and the discharge. The parts of the model which are observed are made of transparent Plexiglass material.

In the model,  $H_1$  represents the reservoir water level,  $h_2$  the water level in the gate,  $h_3$  shows the water level in gate chamber and  $H_4$  shows the tail water level. Cross sectional tunnel height and gate opening are represented by  $e_0$  and  $e$ , respectively. The upstream part, from reservoir to gate, is named as the intake structure, area near the gate is named as gate area and the distance from gate to turbine valve is named as the penstock. The details of the gate region are shown in Figure 2.3.

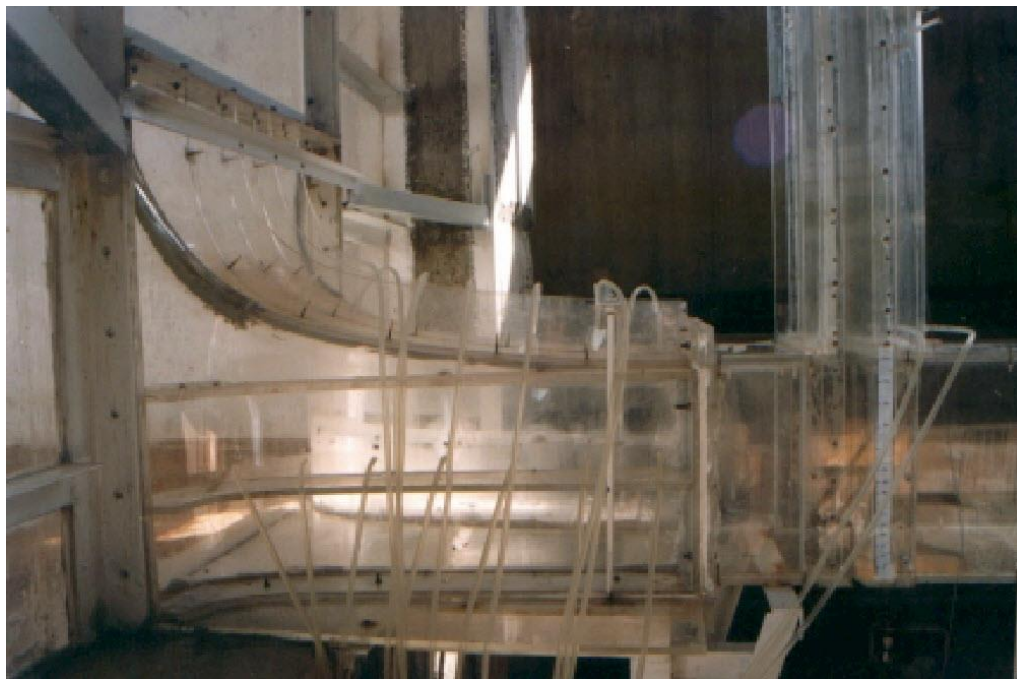


Figure 2.1 Views from hydraulic model (Aydin et al., 2003)

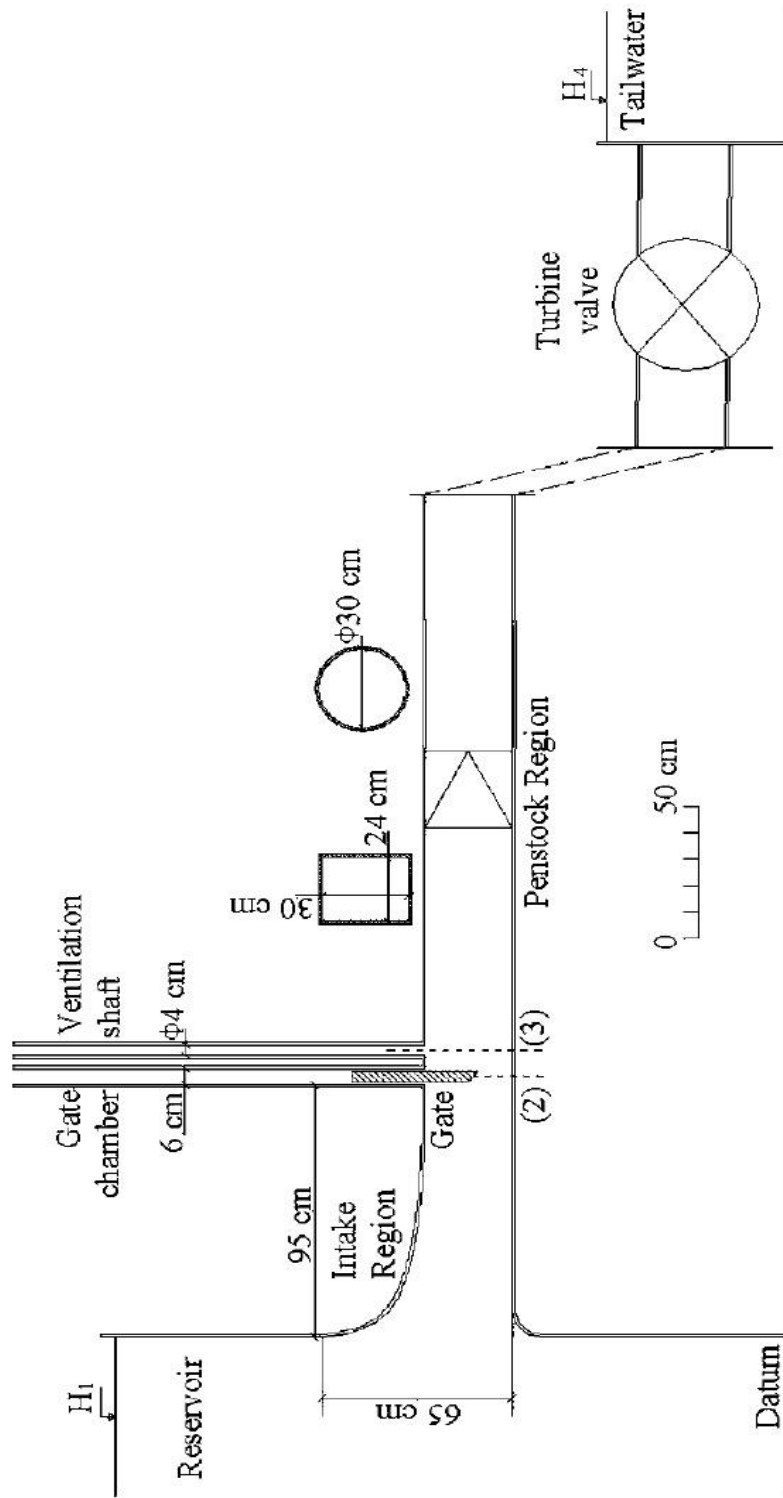


Figure 2.2 Experimental setup (Aydin et al., 2003)

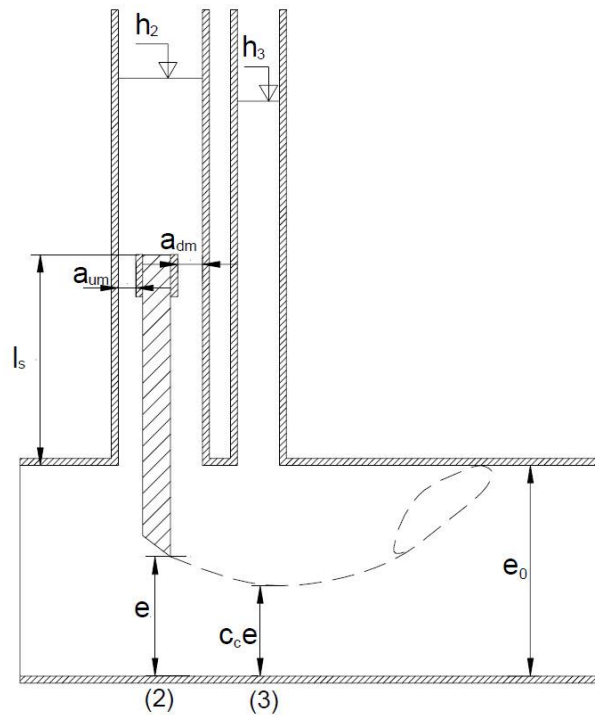


Figure 2.3 Details of gate region (Aydin et al., 2003)

First, water gathered from the elevated tanks was filled up the model reservoir and after it passes through the experimental system, it was redirected to a discharge measurement channel. The water level in the reservoir was maintained by the aid of a channel installed next to the lateral walls of the reservoir. The discharge was set by the help of the valve, which simulates a turbine.

The experiment was carried out with four different gate lips with variable lip angles. The lip angle of the gate can be easily changed by demountable parts. The pressure was measured by five holes connected to copper pipes as shown in Figure 2.4. Pressure transducers were used to measure the pressure from these pipes by the help of manometer tubes (Aydin et al., 2003).

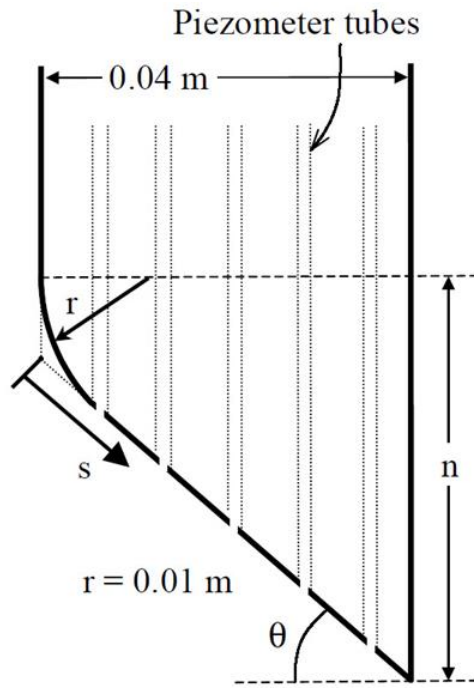


Figure 2.4 Gate lip details (Aydin et al., 2003)

Four different lip angles were studied, which are considered to be covering complete practical range and shown in Table 2.1.

Table 2.1 Gate lip angles

Lip Symbol	n (cm)	Lip angle, $\theta$ (degrees)
A	2	26.5
B	3	36.7
C	4	44.7
D	5	51.6

## 2.2 Forces on a Hydraulic Gate

Hydraulic gates with large cross-sectional area are subjected to several forces during their operation. Normal load case of a hydraulic gate generally consists of frictional force, hydrodynamic forces, dead weight, buoyant forces, transit loads and driving forces (Erbisti, 2004).

A fully closed hydraulic gate is balanced in horizontal forces and is only subjected to buoyant forces by means of vertical forces. The hydrostatic balance is disturbed if a hydraulic gate is partially opened and the flow beneath the gate reaches high velocities and reduces the pressure, which causes a non-uniform distribution of piezometric head around the gate. Large hydrodynamic forces occur as these velocities reaches higher values, hence leading an increase in the pressure difference (Erbisti, 2004).

The pressure difference occurring at the gate bottom causes a vertical force, which is called the downpull force. Reducing hoist capacity by minimizing downpull, is the main objective of many gate designers and researchers throughout the years (Sagar, 2000). Gate downpull is determined by using an equation such as:

$$D_P = \gamma_w \cdot K_L \cdot A \cdot H \quad (2.1)$$

where

$D_P$  = Downpull force on the gate

$\gamma_w$  = Specific weight of water

$K_L$  = Downpull force coefficient

$A$  = Cross-sectional area of the gate on horizontal plane

$H$  = Operating head on the gate bottom

### 2.3 Downpull Force Coefficient

Base variables that downpull force coefficient depends on are the lip angle,  $\theta$ , dimensionless gate opening,  $y$  ( $e/e_0$ ) and the system discharge,  $Q$ . If a dimensionless coefficient is used instead of downpull force and Reynolds number for discharge, all variables will become dimensionless. The measured piezometric head distributions are used to estimate this dimensionless downpull coefficient.

$$K_L = \frac{h_2^* - \bar{h}_1}{\frac{U_g^2}{2g}} \quad (2.2)$$

where  $h_2^*$  is the piezometric head just upstream from the gate and  $U_g$  is the average velocity under the gate lip cross section.

$\bar{h}_1$  is defined as the average piezometric head acting on the gate lip and found from the equation;

$$\bar{h}_1 = \frac{\int h_p dA_{hL}}{A_{hL}} \quad (2.3)$$

where  $h_p$  is the piezometric head and  $A_{hL}$  is the horizontally projected area of the gate lip.

## **2.4 Experimental Results**

### **2.4.1 Pressure Distributions on the Gate Lip**

To investigate the variations of the downpull coefficient, five gate openings ( $y=0.1, 0.2, 0.4, 0.6, 0.8$ ) and five different discharge values for each opening were experimented. Pressure distributions on the gate lips were presented as a function of the distance  $s$ , along the inclined gate lip face (in flow direction). Pressure distributions on four different gate lips from experimental study are shown in Figures 2.5, 2.6, 2.7 and 2.8. Because of the flow separation occurrence, it can be seen that the pressure near upstream edge is lower.

The data points shown in the figures are representing the piezometric readings taken from the holes located on the demountable gate lip. Therefore, it should be said that the graphics are based upon five data points only.

During the hydraulic study, the water level in the reservoir was greatly affected by the fluctuations, consequently was subjected to small changes, thus it was difficult to maintain the water level. Therefore it should be noted that the reservoir water level in each experiment which the results are given through Figures 2.5 to 2.8 are not the same.

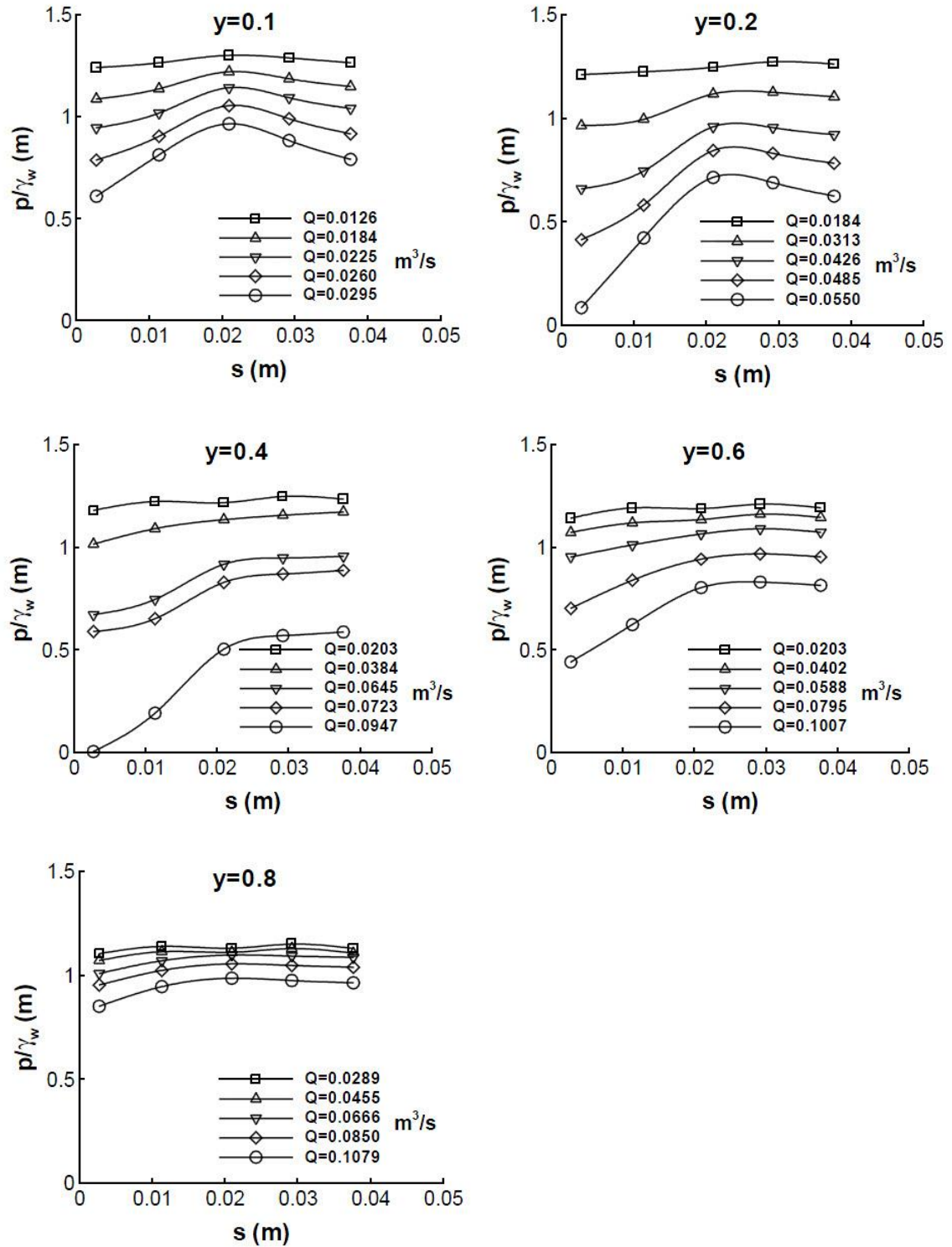


Figure 2.5 Pressure distribution on gate lip, Lip A ( $\theta=26.5^\circ$ ). (Aydin et al., 2003)

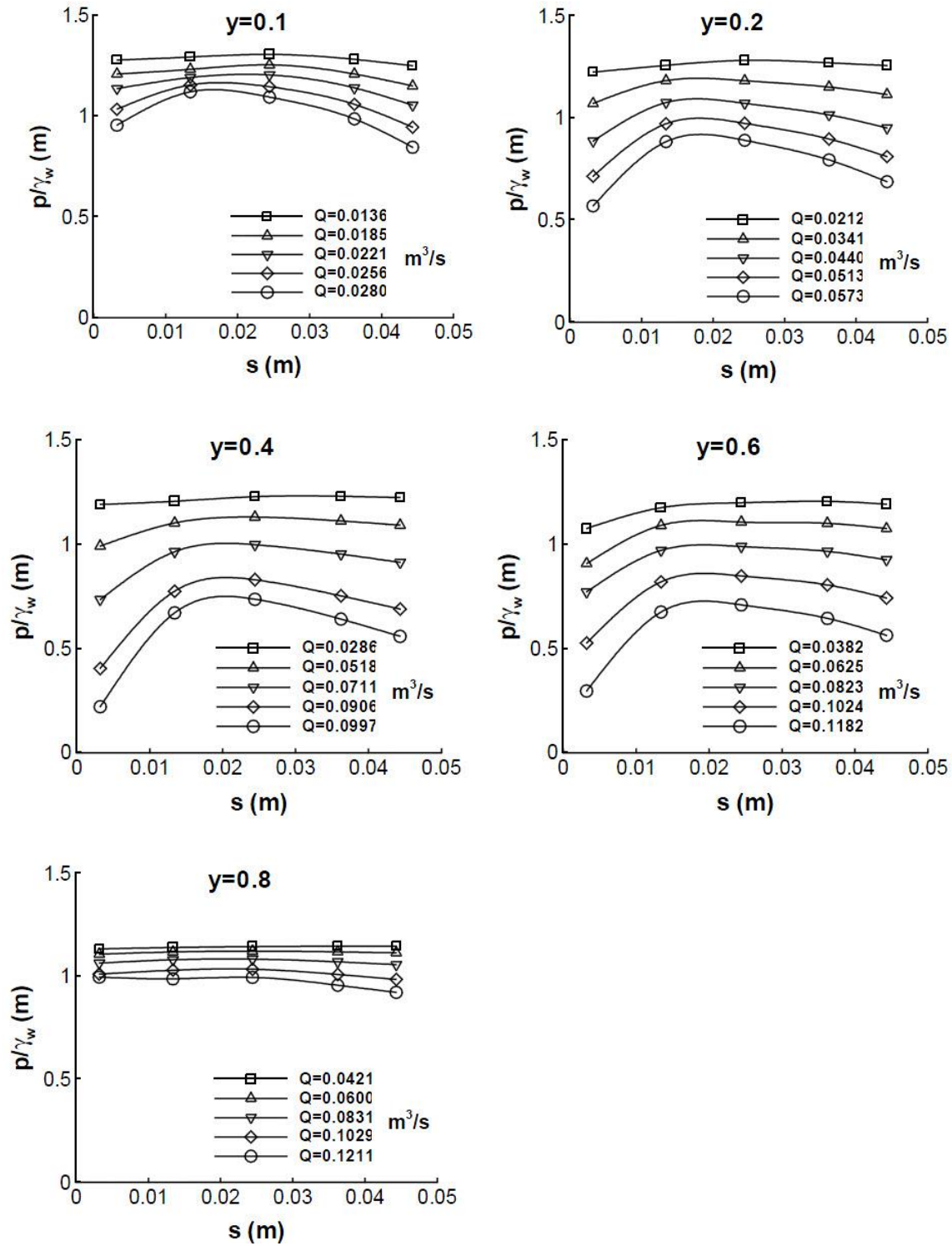


Figure 2.6 Pressure distribution on gate lip, Lip B ( $\theta=36.7^\circ$ ). (Aydin et al., 2003)

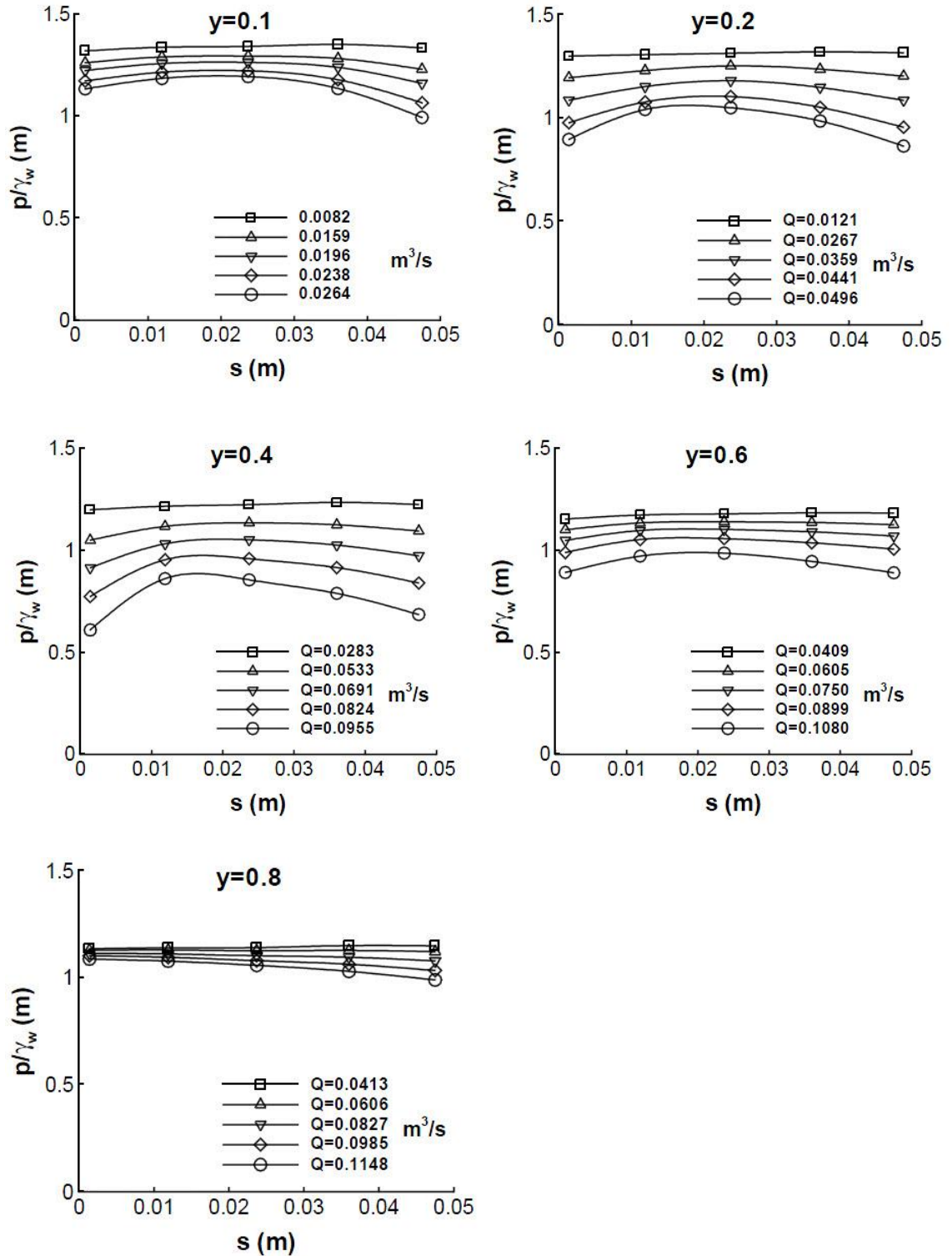


Figure 2.7 Pressure distribution on gate lip, Lip C ( $\theta=44.7^\circ$ ). (Aydin et al., 2003)

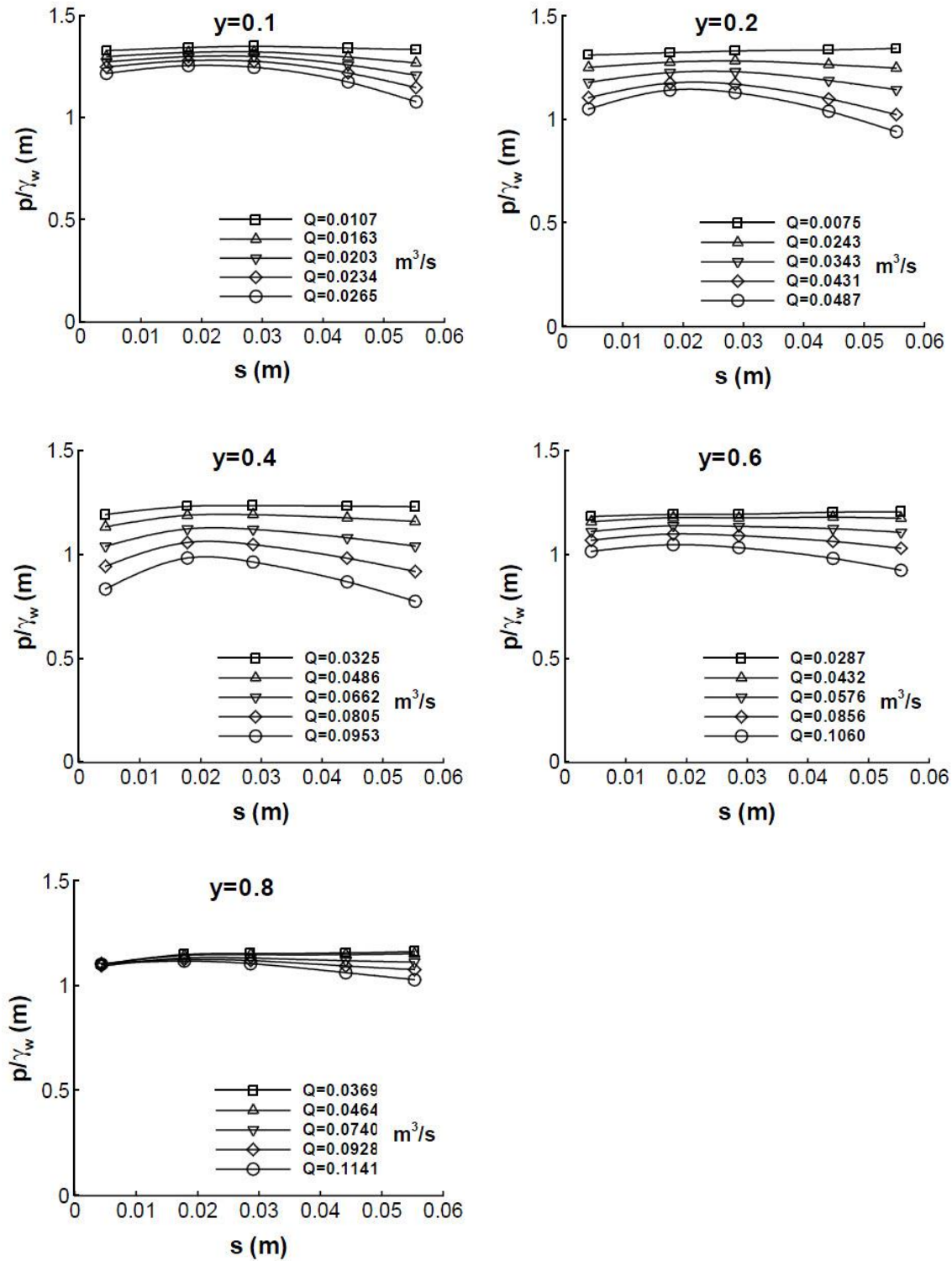


Figure 2.8 Pressure distribution on gate lip, Lip D ( $\theta=51.6^\circ$ ). (Aydin et al., 2003)

### 2.4.2 Lip Downpull Coefficient—Reynolds Number Relationship

It is reported that for cases with the Reynolds number higher than 165000, the downpull coefficient is independent of the Reynolds number (Naudascher, 1991). In the hydraulic study, the effects of Reynolds number on  $K_L$  was investigated by regulating the system discharge by keeping the gate opening constant for different lip angles. Results are presented for five different openings in Figures 2.9, 2.10, 2.11, 2.12 and 2.13. The  $K_L$  value approaches to a constant value asymptotically with increasing Reynolds number. The limiting Reynolds number above which  $K_L$  remains constant, is low for small gate openings, while it becomes higher for larger openings.

If the Reynolds number is assumed to be large enough at all times, which is the case for practical problems, it would be more convenient to state that the  $K_L$  number is independent of the Reynolds number. Then it can be said that the safest way to measure  $K_L$  value is to conduct the experiment with the maximum discharges that the system can pass for each gate opening.

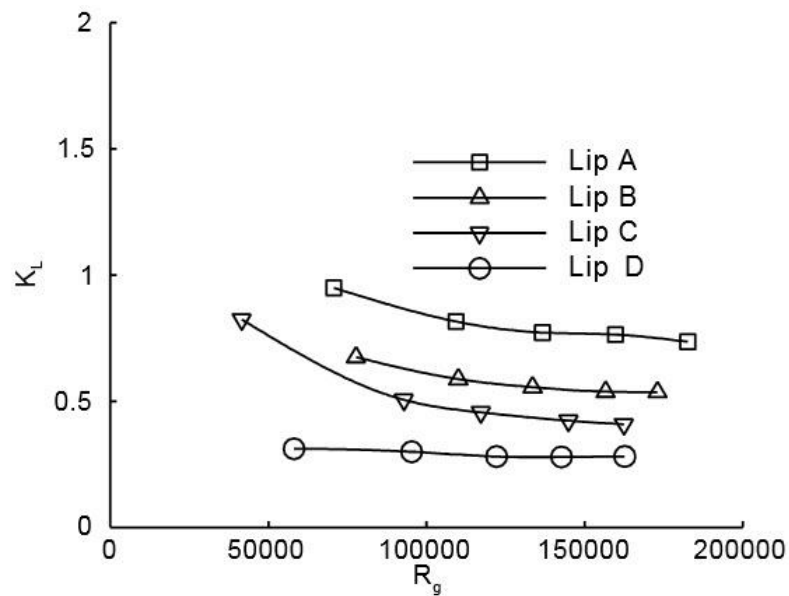


Figure 2.9 Downpull coefficient—Reynolds number relationship,  $y=0.1$  (Aydin et al., 2003)

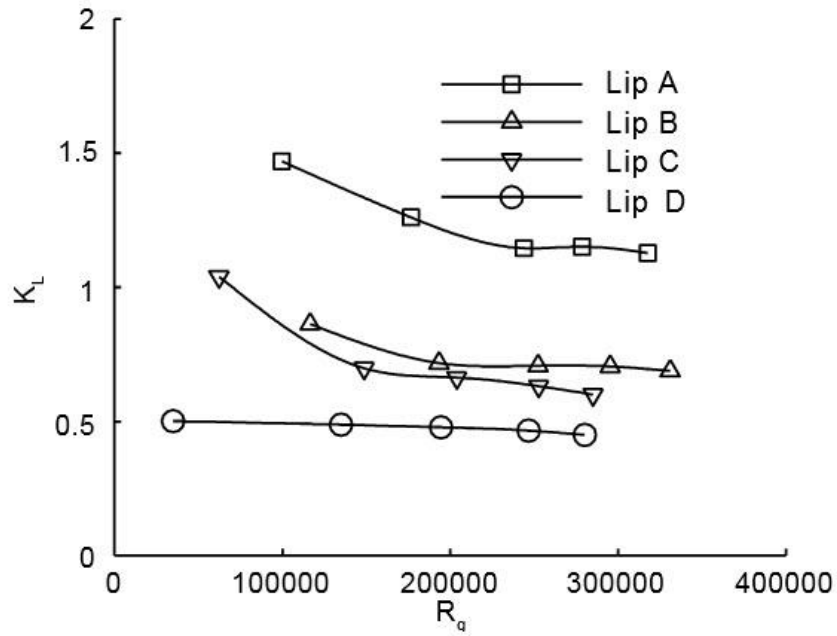


Figure 2.10 Downpull coefficient—Reynolds number relationship,  $y=0.2$  (Aydin et al., 2003)

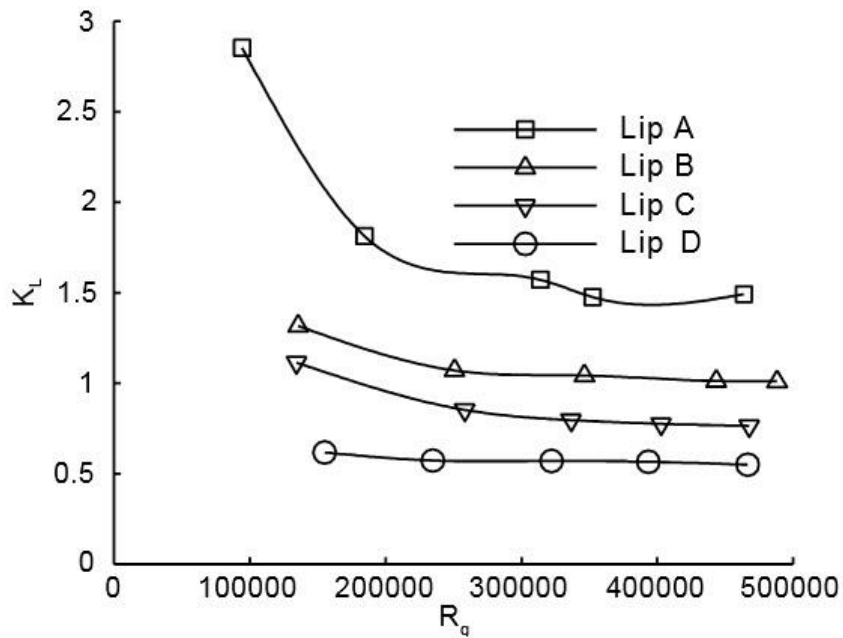


Figure 2.11 Downpull coefficient—Reynolds number relationship,  $y=0.4$  (Aydin et al., 2003)

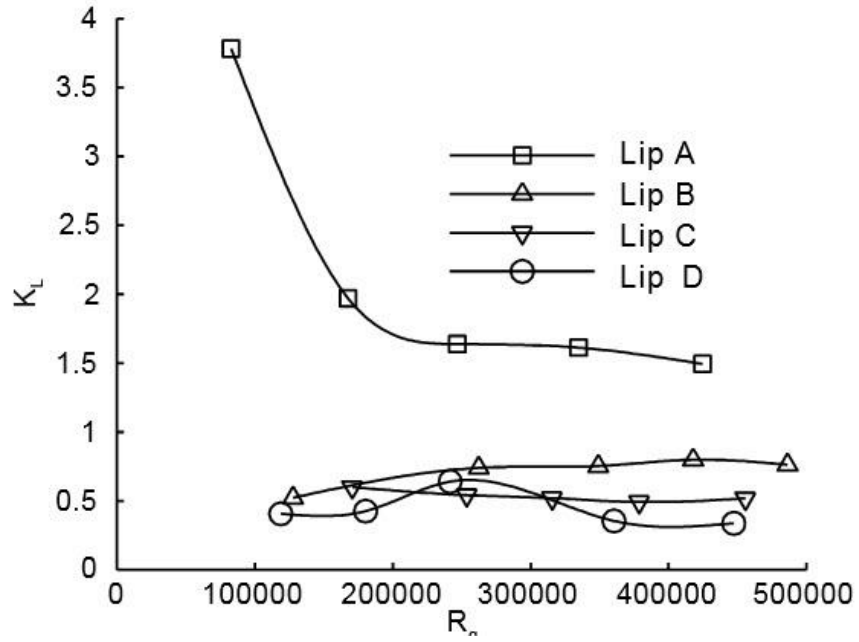


Figure 2.12 Downpull coefficient—Reynolds number relationship,  $y=0.6$  (Aydin et al., 2003)

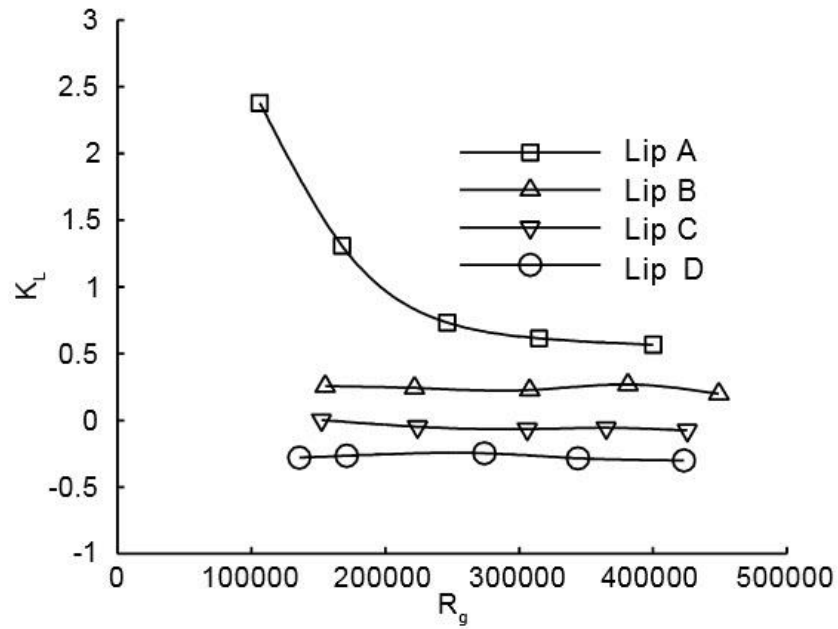


Figure 2.13 Downpull coefficient—Reynolds number relationship,  $y=0.8$  (Aydin et al., 2003)

### 2.4.3 Lip Downpull Coefficient as a Function of the Gate Opening and the Lip Angle

One of the most important outcome of this experimental study is the  $K_L$  coefficient. This coefficient was presented as function of two dimensionless variable, which are lip angle,  $\theta$ , and the dimensionless gate opening,  $y$ , in Figure 2.14.

Ultimately,  $K_L$  was written as a function of the lip angle and gate opening. First,  $K_L$  was stated as a polynomial where  $y$  is the independent variable.

$$K_L = c_1 + c_2y + c_3y^2 + \dots + c_ny^{n-1} \quad (2.4)$$

where  $c_i$  is a function of  $\theta$ . As can be seen from Figure 2.14, curvature changes around  $y=0.8$ . For this reason, the  $K_L$  function was presented as two parts.

For  $0 < y < 0.8$

$$K_L = (14.583 - 0.2296\theta + 0.000355\theta^2)y + (17.111 - 0.3353\theta + 0.01065\theta^2)y^2 + (-0.0974 + 1.772\theta + 0.030452\theta^2)y^3 + (14.246 - 1.394\theta + 0.0217\theta^2)y^4 \quad (2.5.a)$$

For  $0.8 \leq y < 1$

$$K_L = (316.9 - 2.124\theta - 0.03056\theta^2) + (-1485.9 + 4.643\theta + 0.22213\theta^2)y + (2605.9 + 2.708\theta - 0.54872\theta^2)y^2 + (-2006.7 - 12.153\theta + 0.56784\theta^2)y^3 + (569.89 + 6.926\theta - 0.2107\theta^2)y^4 \quad (2.5.b)$$

Equation 2.5 is valid for lip angles larger than  $26^\circ$  and smaller than  $52^\circ$  at every gate opening ( $0 < y < 1$ ). Downpull coefficient can be calculated from Equation 2.5 and then the downpull force on the gate lip can be evaluated.

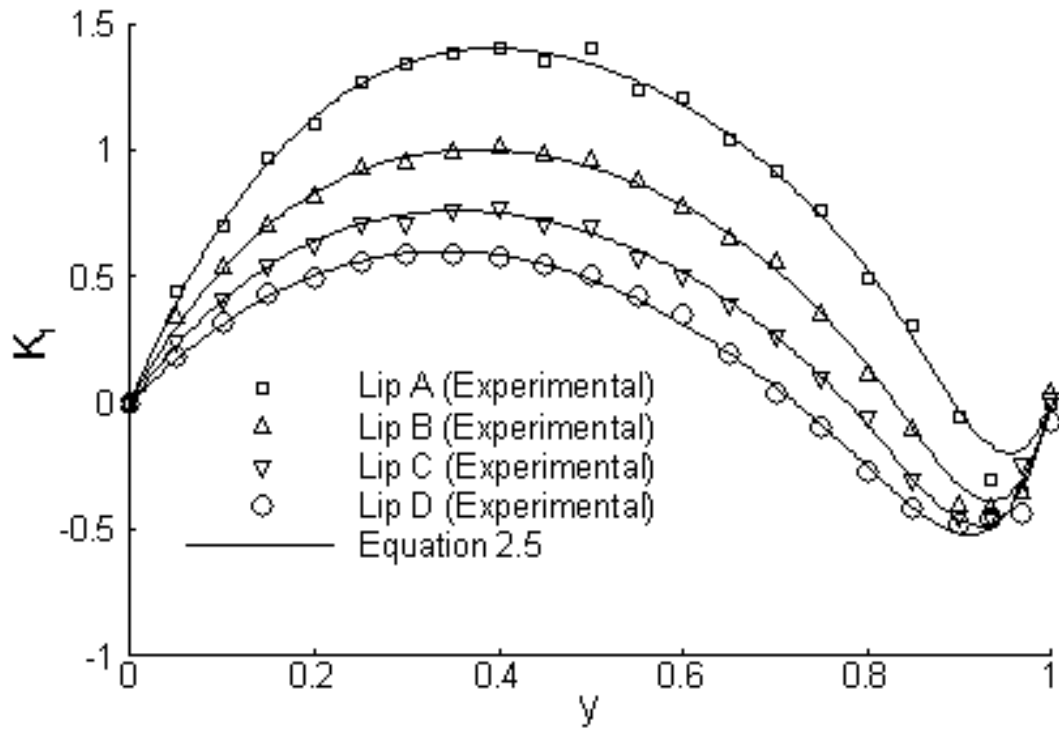


Figure 2.14 Downpull coefficient as a function of gate opening and gate lip angle (Aydin et al., 2003)



## **CHAPTER 3**

### **COMPUTATIONAL MODEL**

GAMBIT v2.4.6 is used for forming the geometry and mesh generation. For simulations, ANSYS FLUENT v14.0 is used as the solver, pre and post processor. The scale of the computational model is selected to be the same as the experimental study.

#### **3.1 Mesh Generation with GAMBIT**

GAMBIT is a geometry and mesh generation software package designed to help analysts and designers build and mesh the models for computational fluid dynamics (CFD) and other scientific applications, usually used with FLUENT. GAMBIT's single interface for geometry creation and meshing brings together most of FLUENT's preprocessing technologies in one environment.

##### **3.1.1 Forming the Geometry**

The general geometry is adapted from the aforementioned experiment. Unlike the full three dimensional experimental model, the system is modelled in 2D. The full domain and final form of the geometry can be seen in Figure 3.1.

The geometry is adapted without the following features;

1. The ventilation chamber is not modelled and is not taken into account. It will be seen later in this thesis that the results are not affected by the presence of the air chamber.
2. Tail water region is not modelled as it was done in the experiment. Details of downstream geometry of the pipe, such as its length, is not specified in the numerical model, since the experiment has its own structure for regulating the flow and a tank where the tail water is accumulated. Since it is hard to define such structure, the region, namely the pipe after the gate, representing the downstream of the gate is kept long enough in the numerical model to avoid any backflow issues.
3. Intake is also modelled in a different way. Since it is needed to obtain a fully developed flow before the gate, an intake structure was built in this experiment as shown in Figure 2.2. However, in this computational study, for the sake of an easy modelling, the intake region is modelled as a straight rectangular duct, and this region is kept long enough for the flow to reach its fully developed state. The upstream region can be defined as the pipe starting from inlet, reaches up to the gate area. The length of the upstream region, along with the downstream length, are decided by numerical experiments and will be discussed later in the thesis.

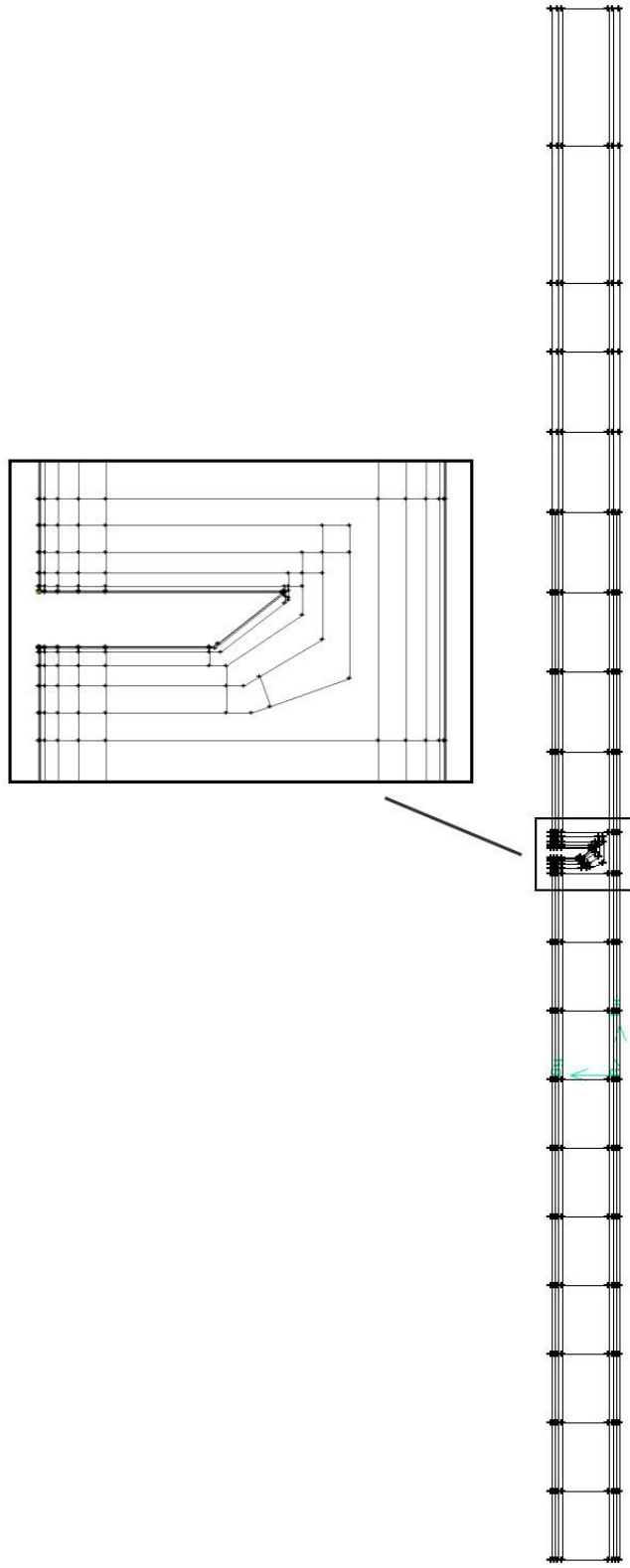


Figure 3.1 Geometry formed by GAMBIT

### 3.1.2 Forming the Grid

As it can be seen from the Figure 3.2, the geometry is generated using block-based modelling. This type of modelling is helpful while forming the mesh, as one can control the number of grid points and the grid size along the boundaries of these blocks.

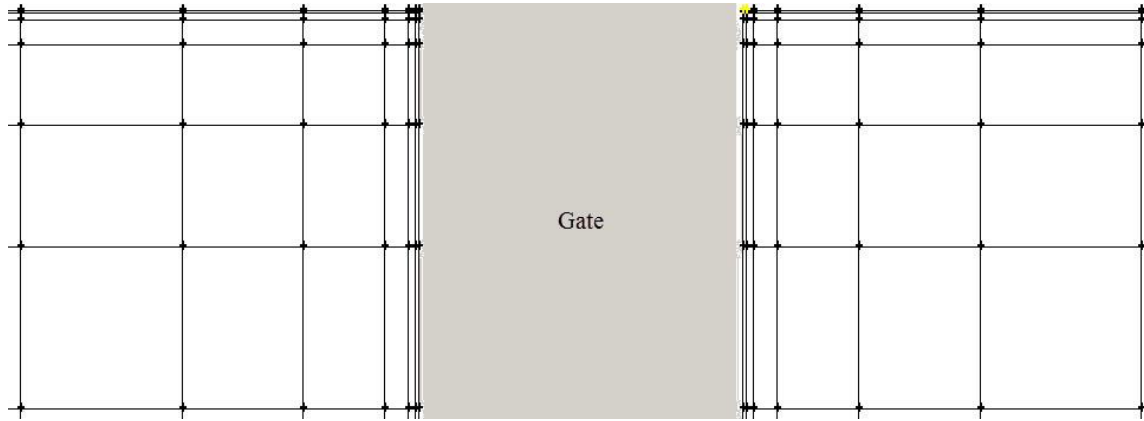


Figure 3.2 Block based modelling

The reason for using block based modelling for the domain can be explained by two elements;

- Since finer grid resolution is required close to the solid boundaries and the grid elements get coarser as it approaches the center of the duct and away from the gate, it is needed to do clustering. The clustering process is not carried out by a uniform ratio, so blocking was considered as an option to control this element enlargement process.
- In case of a need of a re-mesh of a specific part of the model, the block can be re-meshed without the need of changing the non-related mesh in a further area. It is also a time consuming process to re-mesh all the domain once the model is changed. Block based modelling helps for this reason.

### 3.1.3 Clustering

Clustering, also known as grading or refinement can be defined as assigning a progressive spacing between grid points, to change how accurately the solution is wanted to be calculated in that region.

Mesh is refined near walls and clustered by blocks as it gets far away from the walls up to some level as seen in Figure 3.3. Close to the solid walls a structured mesh is used along a small band parallel to the side walls. Then, an unstructured grid is used towards the center of the duct until the coarsening of the mesh is sufficient. A structured mesh is used once again through a large band along the center. Refinement or coarsening are done considering a smooth transition from walls to the center area.

This mesh refinement has been done in all models, in order to gather accurate results near essential areas such as near walls and around the gate and especially gate lip. Since it is desired to obtain the whole mesh with grid points as few as possible, some areas are considered to be less important than these essential areas.

As can be seen from the Figure 3.3, quadrilateral elements are used for meshing. By examining the mesh it can be seen that the quadrilateral mesh has lower skewness which improves quality and convergence rate of the solution. It also gives better control of the mesh, especially near walls.

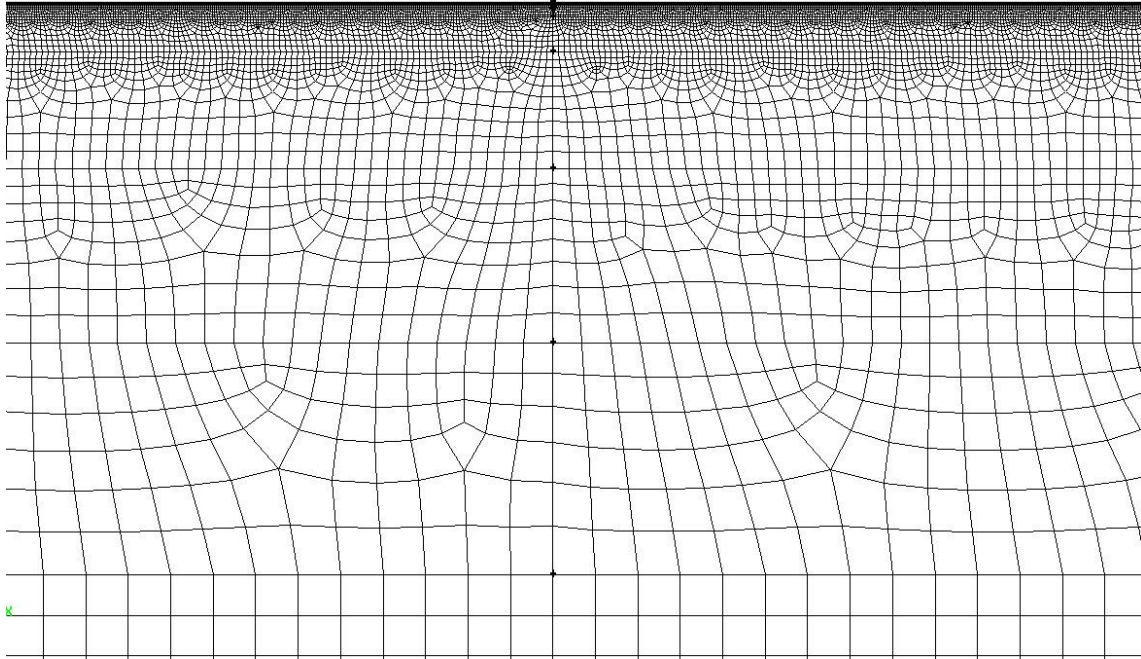


Figure 3.3 Mesh refinement

Since more detailed data with less error is desired from gate lip calculations, the area around the gate lip is meshed finer than the rest of the domain as shown in Figure 3.4.

After completion of meshing of each block, the generated mesh is checked for the quality. The reason behind this check is because properties such as skewness can greatly affect the accuracy and robustness of the CFD solution.

It is not practical to show the complete domain in the thesis. Therefore mesh around the gate, part of the upstream and the transition of the mesh at downstream are shown in Figure 3.5.

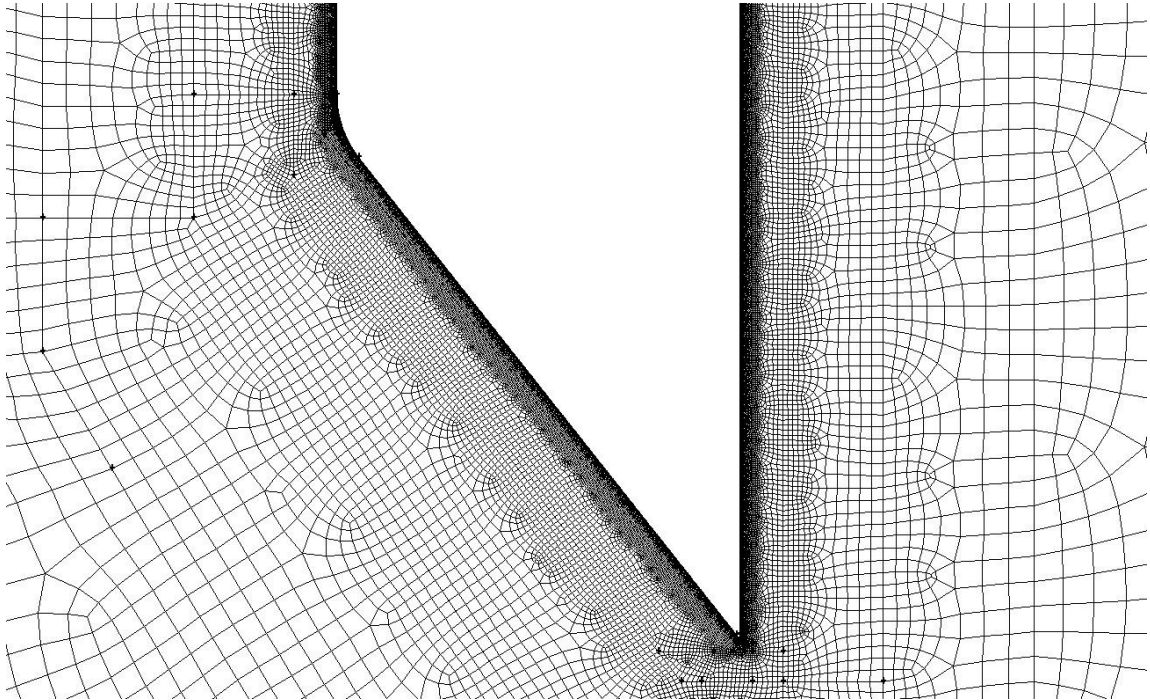


Figure 3.4 Mesh around the gate

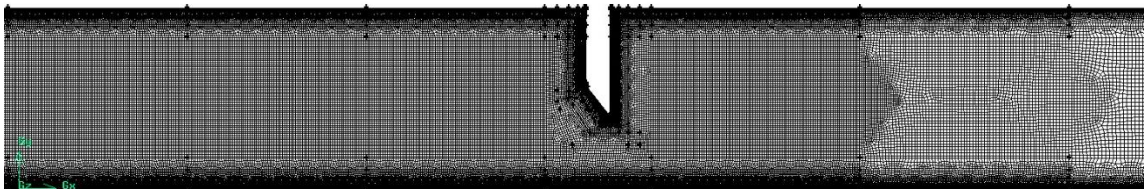


Figure 3.5 Mesh around gate and parts of upstream and downstream

### 3.1.4 Near Wall Mesh

In order to calculate the shear stresses and velocity profiles near wall precisely, structured mesh is generated near walls, where the grid lines are perpendicular to the walls.

The geometry is modelled considering the near wall treatment. The mesh is stretched near the walls so that the first grid point always falls inside the viscous sublayer.

Approximately 10 grid points were used in the wall normal direction up to the logarithmic region where the non-dimensional distance to the wall is approximately 30 wall units ( $y^+ \sim 30$ ). A sample mesh showing this property can be seen from Figure 3.6.

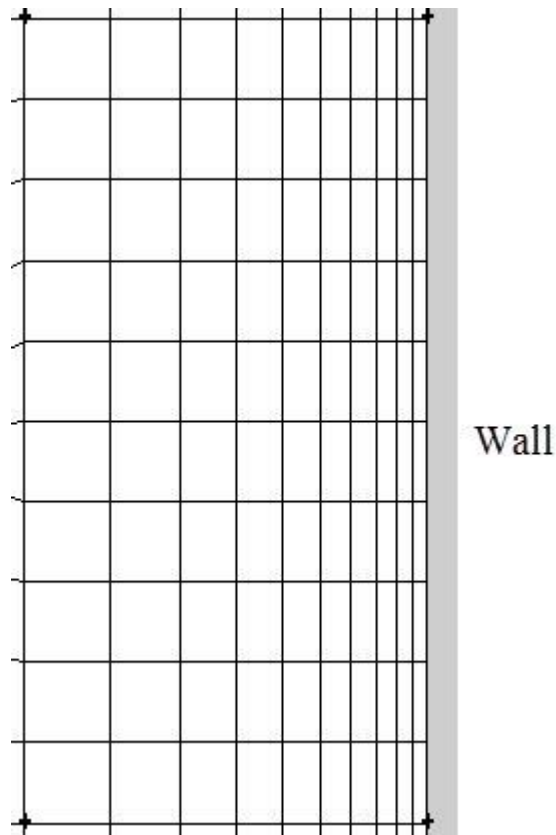


Figure 3.6 Near-wall mesh

### 3.1.5 Mesh Size

The size of the mesh varies for each model, depending on the geometry of the gate. The number of grid points is about 1.1 million for small gate lip angles, whereas it scales up to 1.3 million for larger gate lip angles. This variation is coming from the difficulties experienced while meshing around the gate for larger gate lip angles. In addition, the projectile area under the gate lip that needs to be meshed is larger in large angles.

### **3.1.6 Boundary Conditions**

The inlet section of the model is defined as “Velocity Inlet” and the outlet section is defined as the “Pressure Outlet”. All boundaries, including the gate except inlet and outlet are defined as “Wall” in GAMBIT. More information about the boundary conditions are explained in the following sections.

## **3.2 ANSYS FLUENT Setup and Simulations**

For simulations, ANSYS FLUENT is used. FLUENT is a state-of-the-art computer program, written in C programming language for modeling fluid flow in complex geometries and a variety of applications.

The mesh is transferred from GAMBIT. The procedure for a typical simulation is shown step by step in the following sections.

### **3.2.1 Importing the Mesh**

The mesh imported from GAMBIT to FLUENT. FLUENT automatically recognizes the mesh and the boundary conditions, as these software are compatible with each other.

### **3.2.2 Scaling, Defining the Material and Gravity**

Before being used, the system is scaled by an integrated scale function, since all GAMBIT models are generated using centimeters, whereas meter is used as the length unit in FLUENT. After that, water is defined as the material in the pipe and the zone is set to be all water. Water is defined from the integrated database of FLUENT and the properties are shown in Table 3.1.

Table 3.1 Material definition

Material	Density	Viscosity
water-liquid (h2o<l>)	998.2 kg/m <sup>3</sup>	0.001003 kg/m·s

The operating pressure of the system is set to be atmospheric pressure, which is 101325 Pascal, since the system is open to the atmosphere from the outlet. The gravity is set as 9.81 m/s<sup>2</sup> acting in –y direction. It should be noted here that whether the model is solved with or without gravity calculations, entering gravitational acceleration coefficient has a negligible effect on the general solution of the problem.

### 3.2.3 Turbulence Model

For turbulence modelling, k-epsilon turbulence model is used with the option “Enhanced Wall Treatment”, because, as mentioned, near wall treatment is considered while generating the computational grid. Enhanced wall treatment is a near-wall modeling method that combines a two-layer model with enhanced wall functions. This option requires that the mesh is to be fine enough near walls, to resolve the laminar sublayer. Default option, which is the standard wall function is applicable in geometries meshed with no near wall considerations. However it is not considered to be an advisable option, since the degree of fineness, particularly near walls, is important especially in complex geometries with high Reynolds numbers. Inputs for turbulence modelling is given in Table 3.2.

Table 3.2 Turbulence model

<b>Turbulence Model</b>				
<b>Model</b>		<b>k-epsilon Model</b>	<b>Near Wall Treatment</b>	
k-epsilon		Standard	Enhanced Wall Treatment	
<b>Model Constants</b>				
<b>C<sub>mu</sub></b>	<b>C1-Epsilon</b>	<b>C2-Epsilon</b>	<b>TKE Prandtl Number</b>	<b>TDR Prandtl Number</b>
0.09	1.44	1.92	1	1.3

### 3.2.4 Boundary Conditions

The boundary conditions were already declared in GAMBIT, which are the “Wall”, “Velocity Inlet” and “Pressure Outlet”, but the actual values should be defined in FLUENT.

In the experimental model, the flow is coming to the intake from a reservoir. It is not practical to model a reservoir in FLUENT, so the boundary condition, “Pressure Inlet” is defined as the inlet boundary, by changing the original condition defined in GAMBIT, which was “Velocity Inlet”. The gauge pressure value is set to be the same for every case, which is 9810 Pa, representing 1 meter of water head. The reason for setting the same value for each case is to simulate a reservoir at the upstream and eliminate the fluctuation effects with maintaining an unchanging upstream water level for different gate openings or gate lips. At this point, it can be said that the problem faced with the experimental model while maintaining the reservoir water level, is not an issue in computational model.

The average velocity through a pipe section is calculated from the given experimental discharge values. For future comparisons, the model is planned to run by the velocity values coming from the experimental data, however, a problem arises while defining a velocity throughout the domain. It is only possible to define a velocity at the inlet in FLUENT because there is not a velocity outlet boundary condition option in FLUENT.

This problem is solved by defining a boundary condition “Velocity Inlet” at the outlet of the domain and entering the velocity value as negative, again by changing the original condition defined in GAMBIT, which was “Pressure Outlet”. This process forces the FLUENT to maintain the desired flow rate throughout entire domain.

Rest of the boundaries are left as “Wall”. Even if these boundaries was not defined, FLUENT automatically detects that these locations should be set as a wall. Yet, all walls were labeled differently for easy extraction of values, such as gate lip, which is named separately and extracted to find pressure values isolated from its surroundings. Walls are defined as stationary walls with no slip shear condition with the default wall roughness coefficients which are given in Table 3.3.

Table 3.3 Wall roughness properties

<b>Wall Roughness</b>	
Roughness Height (m)	0
Roughness Constant	0.5

### **3.2.5 Residuals**

As the code iterates, "residuals" are calculated for each flow equation. These residuals represent a kind of average error in the solution – if a predefined maximum residual is set to be smaller, convergence takes more time. FLUENT checks five different convergence residuals on each step of this iterative process. These residuals are for continuity, x-velocity, y velocity, k and epsilon. The maximum residual criteria value is set to  $10^{-6}$ . This value is tested to be sufficient to achieve a converged solution.

After scaling, setting gravity, the type of turbulence model, defining the material, setting zone conditions, residuals, and boundary conditions, the system is initialized from the outlet for faster convergence, the average velocity magnitude is set initially throughout

the whole flow domain. After initializing the setup, the simulation is run until desired residuals are reached.

### 3.2.6 Simulations

The simulations carried out for each case until the desired residuals have been reached. The average run time of a single model to reach that residuals, varies between 3 to 6 hours with a computer with configurations given in Table 3.4.

Table 3.4 System configurations

Processor	1.6 GHz Intel Core i7 720QM
Memory	6GB, 1066 MHz DDR3
Chipset	Intel HM55

Iteration count and simulation time depends on the gate opening and the discharge. For smaller openings, the run time takes longer compared to the larger opening of gates. For example, for  $y=0.2$  opening model, where  $y$  is the ratio of the gate opening to the height of the gate, the iteration count is around 7000 to reach the maximum residual, where in  $y=0.4$  it is around 5000. A typical iteration vs. residual count is shown in Figure 3.7. It is seen that residuals experiences a quick drop at the beginning of the iterations, then they continue to drop until all of the residuals reach or pass below the desired maximum residual value. Once all residual criterion is achieved for all of the five residuals, the simulation is stopped and the model becomes ready for post-processing.

For some selected models, simulation is run for further 1000 iterations for investigating if further iterations has any effects on the solution. It is found out that the effects of further iterations are negligible after reaching the predefined residual of  $10^{-6}$ .

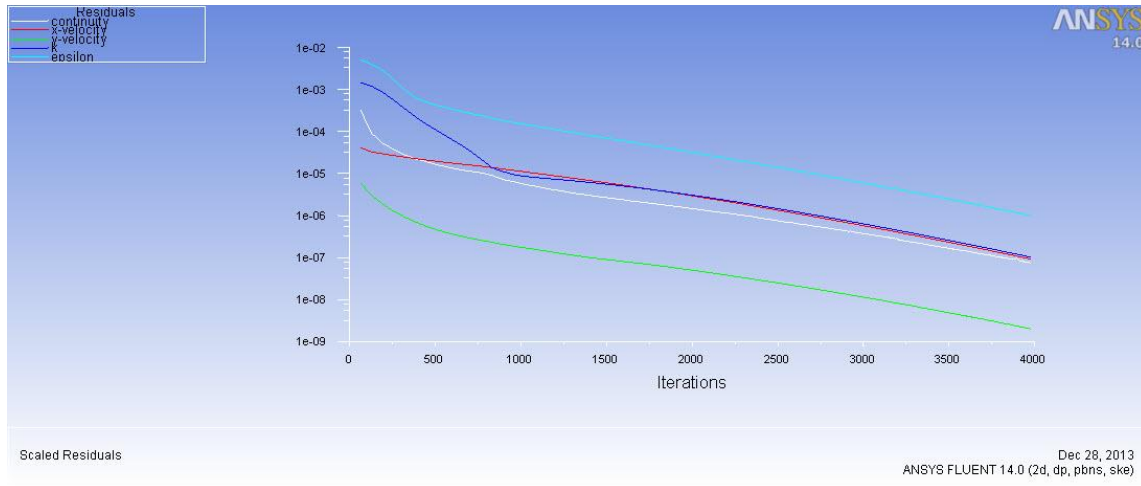


Figure 3.7 Residuals

### 3.3 Selecting the Domain Size

The downstream and upstream part of the system can be defined as the domain part before the gate and after the gate, respectively. It is noted that the downstream part should be long enough to overcome backflow issues, and the upstream should be long enough to develop a fully developed velocity profile. The length of these parts are decided by trial and error. The system is modelled and solved for different lengths of these parts and then a model size is selected and the rest of the simulations are carried out using that length.

The main purpose of these trials is to have a mesh of small size as much as possible. Calculation time is significantly decreased if a smaller mesh size is used.

Trials are carried out using different lengths for the upstream and the downstream part. The trials are started from 6 times duct height upstream and 16 times duct height downstream, where the duct height is 30 cm, and the domain is meshed accordingly. The upstream part is elongated by increments of 2 duct heights ( $2e_0$ ), while keeping the length of the downstream part constant. These tests are done for two different gate openings with maximum discharge that they can pass. The trials done for selecting the length of the

upstream for two gate openings and discharges are given in Table 3.5. The same procedure is done for the downstream part. The downstream part is also elongated by  $2e_0$  increments, but this time keeping the length of the upstream part constant. Tests for selecting the length of the upstream are done for the same two different gate openings with maximum discharge that they can pass. The trials done for selecting the length of the downstream for two gate openings and discharges are given in Table 3.6.

After simulations carried out by FLUENT, results are compared. After comparing the  $K_L$  values,  $10e_0$  and  $12e_0$  is decided to be the most suitable length at the upstream and downstream, respectively.

Table 3.5 Variation in  $K_L$  for different upstream lengths

Case	$y=0.2, \theta=44.7^\circ, Q=0.0496 \text{ m}^3/\text{s}$			$y=0.4, \theta=44.7^\circ, Q=0.0955 \text{ m}^3/\text{s}$		
Lengths (u/s-d/s)	$6e_0-16e_0$	$8e_0-16e_0$	$10e_0-16e_0$	$6e_0-16e_0$	$8e_0-16e_0$	$10e_0-16e_0$
$K_L$	0.63204	0.62719	0.62396	0.76721	0.76262	0.75975
% deviation		0.77192	0.51874		0.60068	0.37899

Table 3.6 Variation in  $K_L$  for different downstream lengths

Case	$y=0.2, \theta=44.7^\circ, Q=0.0496 \text{ m}^3/\text{s}$				$y=0.4, \theta=44.7^\circ, Q=0.0955 \text{ m}^3/\text{s}$			
Lengths (u/s-d/s)	$10e_0-12e_0$	$10e_0-14e_0$	$10e_0-16e_0$	$10e_0-18e_0$	$10e_0-12e_0$	$10e_0-14e_0$	$10e_0-16e_0$	$10e_0-18e_0$
$K_L$	0.62396	0.62396	0.62396	0.62396	0.75973	0.75974	0.75975	0.75975
% deviation		0.00004	0.00004	0.00002		0.00048	0.00052	0.00053

The reason for selecting  $10e_0$  and  $12e_0$  lengths can be seen by looking at the error percentages which are getting smaller as an optimum mesh is reached. After selecting  $10e_0$  and  $12e_0$  lengths, all the simulations are carried out using these lengths.

### **3.4 Grid Dependence Study**

For investigating the effects of the grid size on the solution, a sample GAMBIT model is re-meshed with two different meshes by lowering and increasing the size of the grid. Then, these models are solved by FLUENT and the  $K_L$  value is compared.

Lip angle  $\theta=44.7^\circ$  (Lip C) with  $y=0.4$  gate opening is selected as the geometry to be used in the grid dependence study. The selected model has 1265568 grid points before modification. The mesh is lowered to 827598 grid points, where the percentage of decrease is about 35%. Mesh increase is done to the same model by increasing the grid points to 1625707, with the percentage about 28%. Largest possible discharge value for the opening is selected for the simulations, which is  $0.0955 \text{ m}^3/\text{s}$ .

The comparison of  $K_L$  values and the number of grid points for these two models are given in Table 3.7.

It is seen that lowering the mesh size by 34.6%, ends up with a 4.96% change in the  $K_L$  value and increasing the mesh size by 28.5%, ends up with a 0.22% change in  $K_L$  value. The change in the value obtained from lowering the mesh size, can be seen as an error percentage which may likely alter the solution or gives incorrect results. By increasing the mesh, it is seen that the change in the  $K_L$  value is too small and can be considered as insignificant.

Therefore, throughout this thesis, all models are generated using the mesh of Model 1.

Table 3.7 Grid points and  $K_L$  comparison

	Grid Points	Percentage relative to the Original Model (Grid size)	$K_L$	Percentage relative to the Original Model ( $K_L$ )
Model 1	1265568		0.7597	
Model 2	827598	-34.61	0.7220	-4.96
Model 3	1625707	+28.46	0.7614	+0.22

### 3.5 Computational Results

#### 3.5.1 Processing for Results

After simulations have been done, the static pressure on the gate lip is extracted from FLUENT to a spreadsheet file. This file shows the static pressure on each node located on the gate lip. After extracting this file, Equation 2.3, which is mentioned in the definition of the downpull force coefficient is used to find head loss.

$A_{hL}$ , which is the projected area of each element along the gate lip, is found by subtracting the neighbor x coordinates and taking their median whereas  $h_p$ , the piezometric head is found by dividing the static pressure to specific weight of water.

$h_2^*$ , is defined as the piezometric head just upstream from the gate, that is the reservoir head minus the entrance losses. Since the entrance losses have to be excluded for all the cases investigated, an additional simulation without the gate is modelled and solved using the same boundary conditions. The head losses due to friction coming from the presence of the gate is eliminated by this type of approach. The static pressure value at the location

where the gate was used to be, is read from the FLUENT solutions and divided by specific weight to find  $h_2^*$ .

$U_g$ , which is the average velocity under the gate is also calculated from FLUENT for each case. A vertical interface is defined at the desired location, which is the area under the gate, and the average velocity is found by extracting area-weighted average.

$\bar{h}_1$  is calculated by integrating the piezometric head (denoted as static pressure over specific weight in FLUENT) over the horizontally projected area of the gate lip. This calculation is carried out for each grid point and corresponding projected element area and the summation is made out using Microsoft Excel.

After revealing all unknowns,  $K_L$  is calculated using Equation 2.2.

### **3.5.2 Computational Models**

Compared to the experimental study, number of measured data points are much more in the computational study, which gives an opportunity to monitor small changes of pressure on the gate lip. Data is recorded for each grid point located on the gate lip, which starts from the beginning of the curved part of the gate lip and ends at the tip of the lip. The number of these grid points varies for each model but for the sake of a clear understanding, it can be said that this number is about 700 on average.

The same experiments are modelled and simulated for the given discharges and gate openings. In addition to the experimental gate openings that were simulated, nine more gate openings ( $y=0.3$ ,  $y=0.5$ ,  $y=0.7$ ,  $y=0.85$ ,  $y=0.90$ ,  $y=0.95$ ,  $y=0.97$ ,  $y=0.98$ ,  $y=1.00$ ) are solved for a maximum discharge that the system can pass for each gate opening. These discharges are selected from the proposed maximum discharge curve from the experimental study. Maximum discharge is given as a function of gate opening in Figure 3.8, which is taken from the experimental study (Aydin et al., 2003).

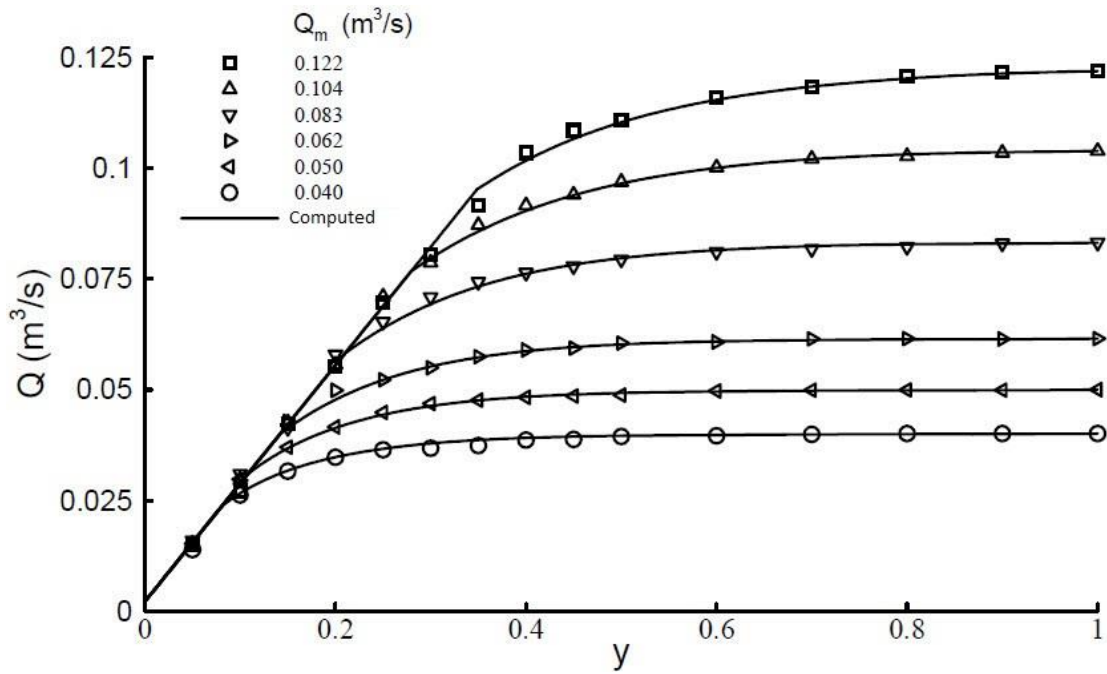


Figure 3.8 Maximum system discharge (Aydin et al., 2003)

All model simulations which are done throughout this thesis are presented in Table 3.8 and Table 3.9. In addition to the ones summarized in these tables, additional simulations are also carried out for the models without the presence of the gate. Therefore, the total number of simulations done for this thesis is about 250.

Table 3.8 Simulations carried out ( $\theta=26.5^\circ$  and  $\theta=36.7^\circ$ )

Gate Opening	Q (m <sup>3</sup> /s)									
	$\theta=26.5^\circ$					$\theta=36.7^\circ$				
y=0.10	0.0126	0.0184	0.0225	0.0260	0.0295	0.0136	0.0185	0.0221	0.0256	0.0280
y=0.20	0.0184	0.0313	0.0426	0.0485	0.0550	0.0212	0.0341	0.0440	0.0513	0.0573
y=0.30	0.0800					0.0800				
y=0.40	0.0203	0.0384	0.0645	0.0723	0.0947	0.0286	0.0518	0.0711	0.0906	0.0997
y=0.50	0.1107					0.1107				
y=0.60	0.0203	0.0402	0.0588	0.0795	0.1007	0.0382	0.0625	0.0823	0.1024	0.1182
y=0.70	0.1182					0.1182				
y=0.80	0.0289	0.0455	0.0666	0.0850	0.1079	0.0421	0.0600	0.0831	0.1029	0.1211
y=0.85	0.1194					0.1194				
y=0.90	0.1216					0.1216				
y=0.95	0.1218					0.1218				
y=0.97	0.1219					0.1219				
y=0.98	0.1220					0.1220				
y=1.00	0.1220					0.1220				

Table 3.9 Simulations carried out ( $\theta=44.7^\circ$  and  $\theta=51.6^\circ$ )

Gate Opening	Q (m <sup>3</sup> /s)									
	$\theta=44.7^\circ$					$\theta=51.6^\circ$				
y=0.10	0.0082	0.0159	0.0196	0.0238	0.0264	0.0011	0.0016	0.0203	0.0234	0.0265
y=0.20	0.0121	0.0267	0.0359	0.0441	0.0496	0.0075	0.0243	0.0343	0.043	0.049
y=0.30	0.0800					0.0800				
y=0.40	0.028	0.053	0.069	0.082	0.096	0.033	0.049	0.066	0.081	0.095
y=0.50	0.1107					0.1107				
y=0.60	0.0409	0.0605	0.0750	0.0899	0.1080	0.0287	0.0432	0.0576	0.0856	0.1060
y=0.70	0.1182					0.1182				
y=0.80	0.0413	0.0606	0.0827	0.0985	0.1148	0.0369	0.0464	0.0740	0.0928	0.1141
y=0.85	0.1194					0.1194				
y=0.90	0.1216					0.1216				
y=0.95	0.1218					0.1218				
y=0.97	0.1219					0.1219				
y=0.98	0.1220					0.1220				
y=1.00	0.1220					0.1220				

### 3.5.3 Pressure Distributions on the Gate Lip

Pressure distributions on four different gate lips for five different gate openings at different discharges from computational study are shown in Figures 3.9, 3.10, 3.11 and 3.12.

Since mesh size on the gate lip is very fine, there are approximately 700 data points where all the flow quantities are recorded, remembering that in the experiments data is recorded on only five points along the gate lip. Because of this, sudden changes on the pressure along the gate lip can be captured within the simulations. Pressure values extracted from FLUENT, which are shown in the figures, are “Static Pressure”, representing the piezometric pressure.

It is seen that pressure on the gate lip experiences a sudden drop at the curved part of the gate lip. This drop is more observable at gate openings  $y=0.2$  and  $y=0.4$ . It can also be said that, as the gate lip angle decreases, in other words, as the gate lip becomes more parallel to the duct bottom, this pressure drop becomes more drastic as the flow separations becomes more likely to occur as the gate lip becomes less streamlined. It is also seen that another pressure drop occurs at the tip of the gate lip, as another flow separation occurs at the tip. Unlike the previous observation, this pressure drop is more noticeable for higher gate lip angles.

As it is mentioned in Chapter 2, the water level in the reservoir in experimental study is not same for each model. However, in computational model, the upstream water level is kept constant, which is 1 meter. Therefore, it is not possible to make a one to one comparison for the pressure distributions of experimental study and computational study.

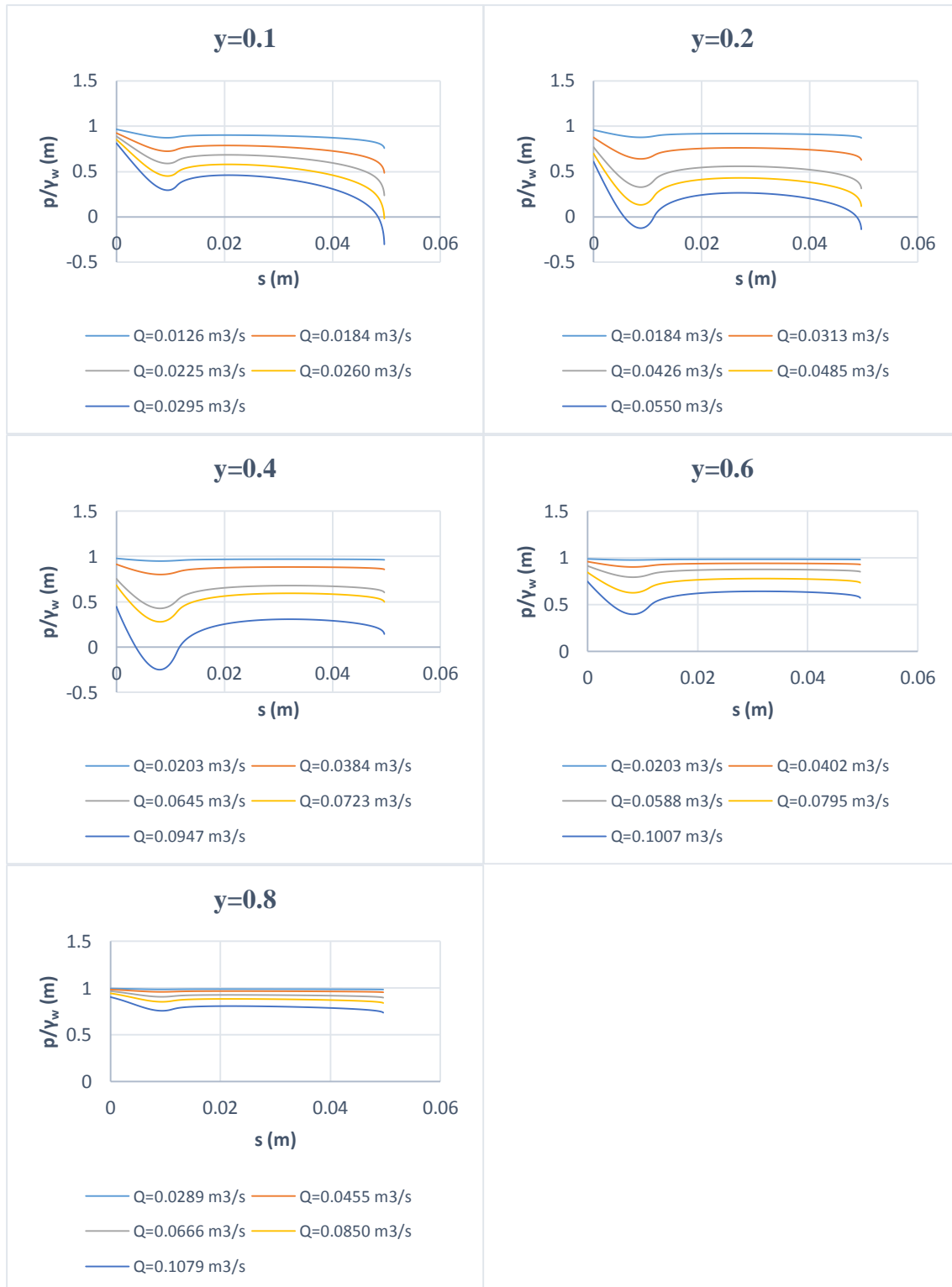


Figure 3.9 Pressure distribution on gate lip, Lip A ( $\theta=26.5^\circ$ ). (Computational)

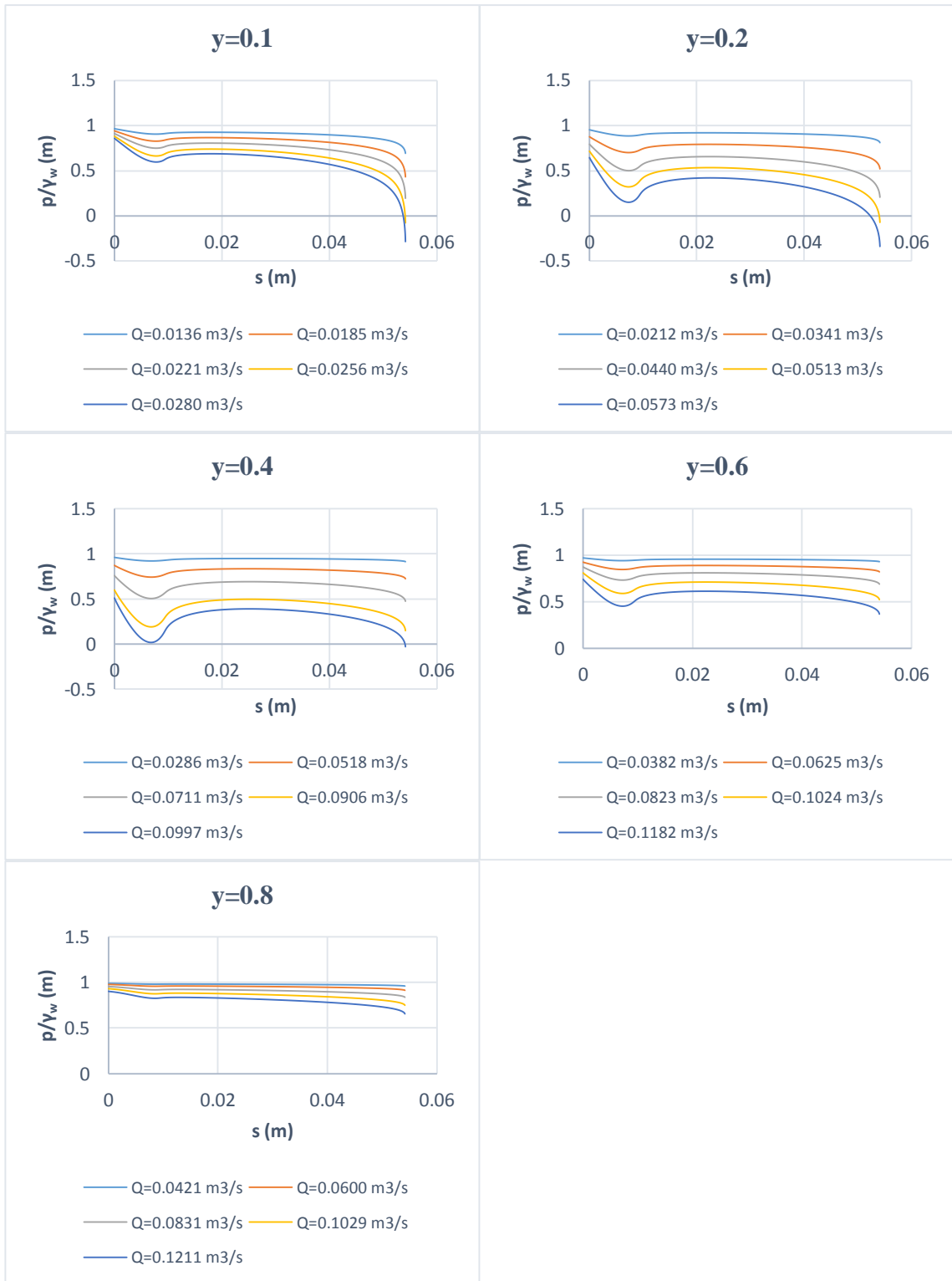


Figure 3.10 Pressure distribution on gate lip, Lip B ( $\theta=36.7^\circ$ ). (Computational)

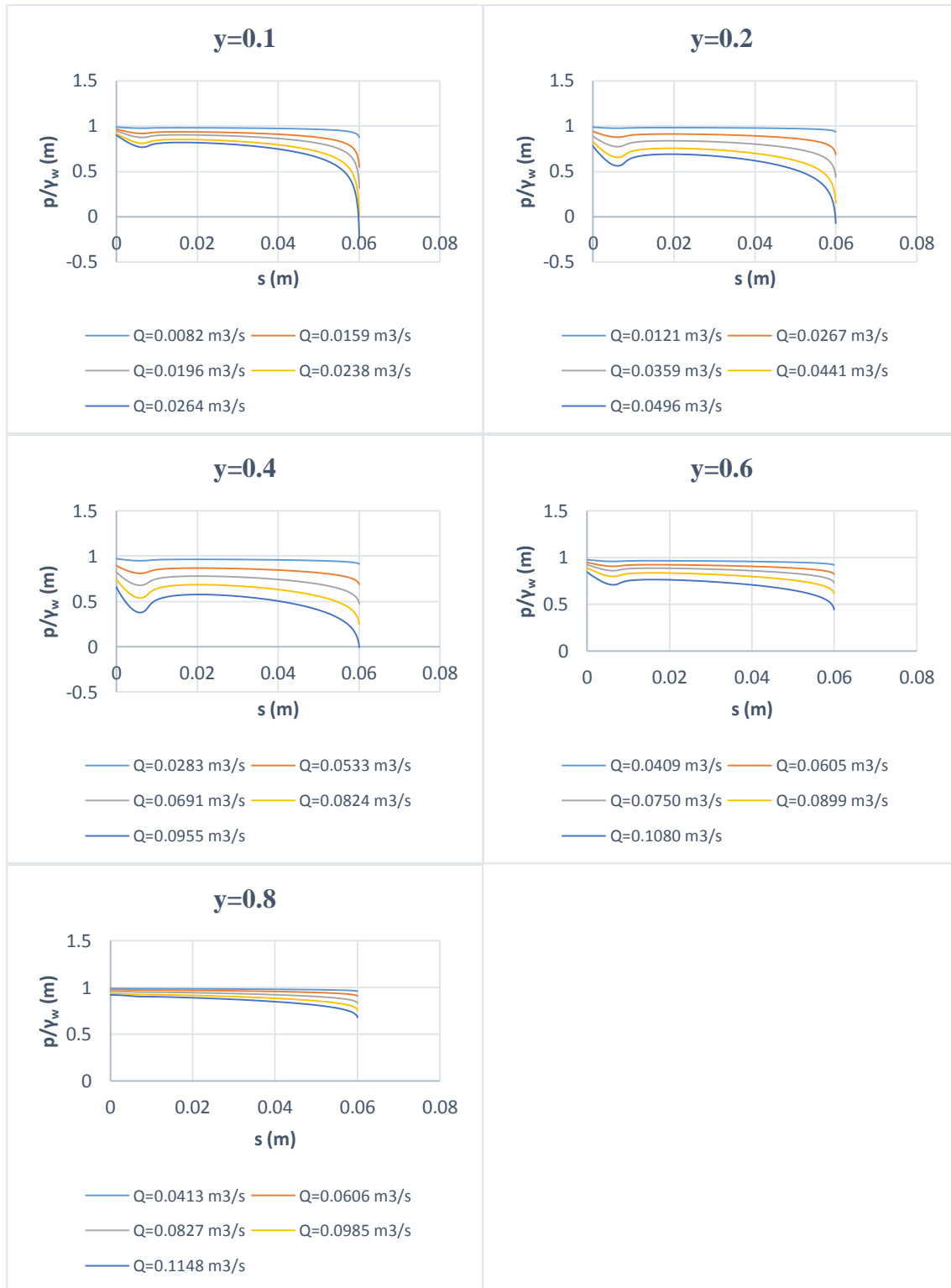


Figure 3.11 Pressure distribution on gate lip, Lip C ( $\theta=44.7^\circ$ ). (Computational)

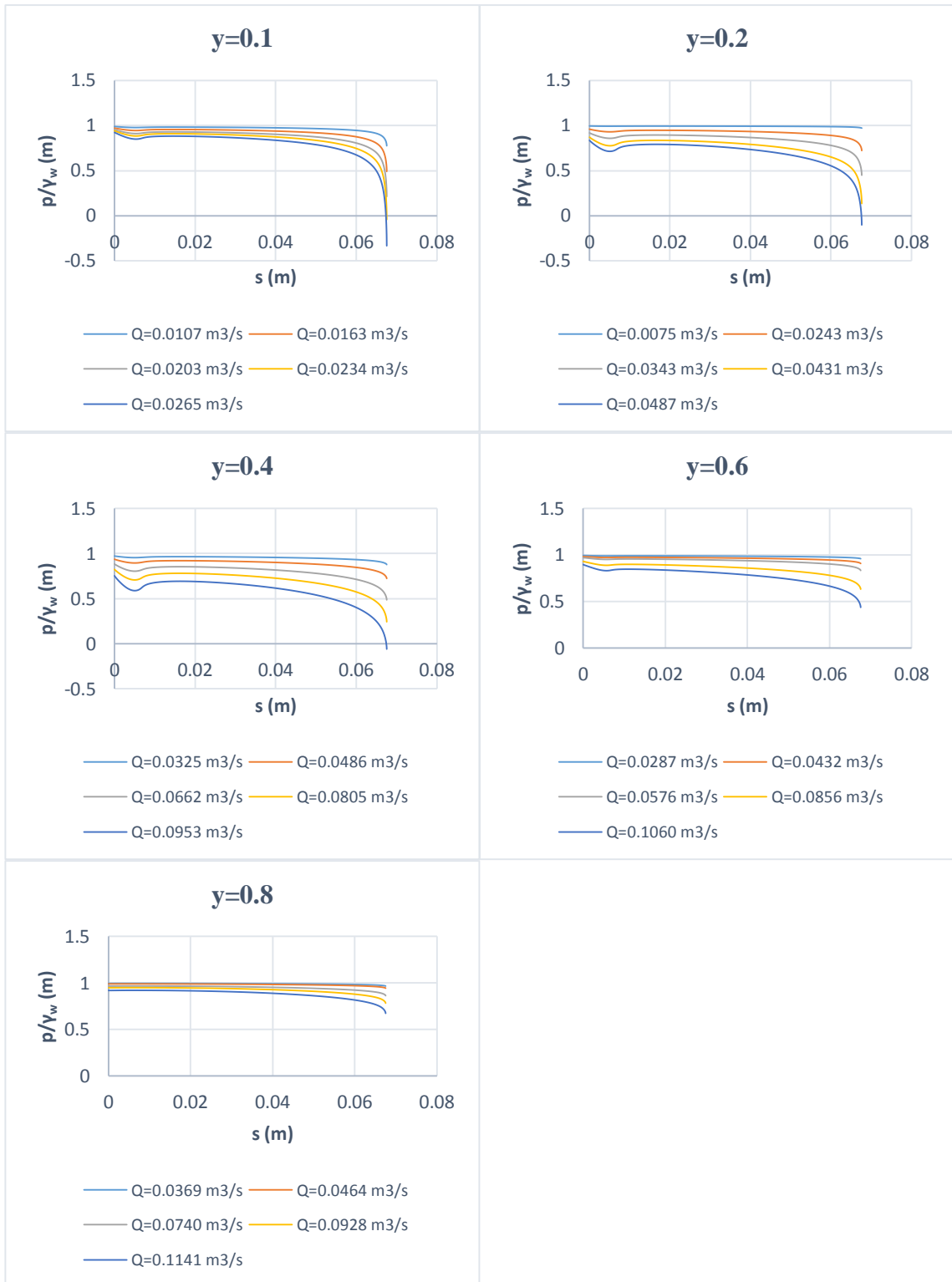


Figure 3.12 Pressure distribution on gate lip, Lip D ( $\theta=51.6^\circ$ ). (Computational)

### 3.5.4 Lip Downpull Coefficient—Reynolds Number Relationship

Variation of lip downpull coefficient,  $K_L$ , with Reynolds number for different lip geometries is obtained from the simulation results and is presented for four different lip angles through Figures 3.13 to 3.17. As it can be seen from these figures,  $K_L$  is always independent of the Reynolds number. Remember that in the experimental study  $K_L$  was independent from Reynolds number only for  $Re > 1650000$ . Flow may have a transitional behavior for low Reynolds numbers and k-epsilon (k- $\epsilon$  for short) turbulence model may not be able to represent this. This may also be related to a steady 2D assumption made in the simulations. It should also be noted that in practical problems the Reynolds numbers encountered are much larger.

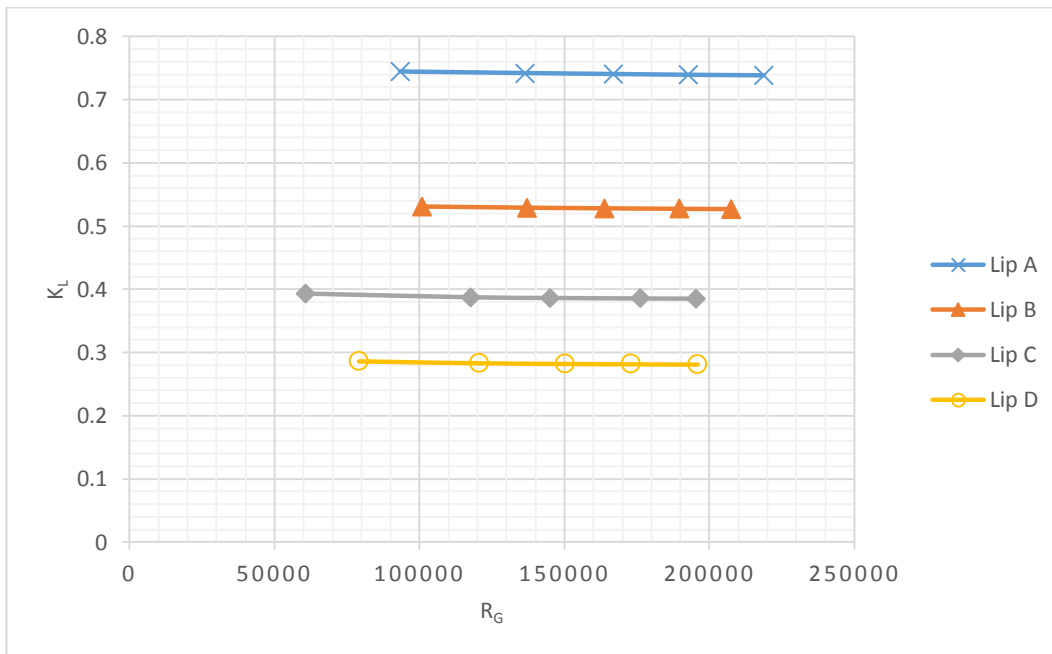


Figure 3.13 Downpull coefficient—Reynolds number relationship,  $y=0.1$  (Computational)

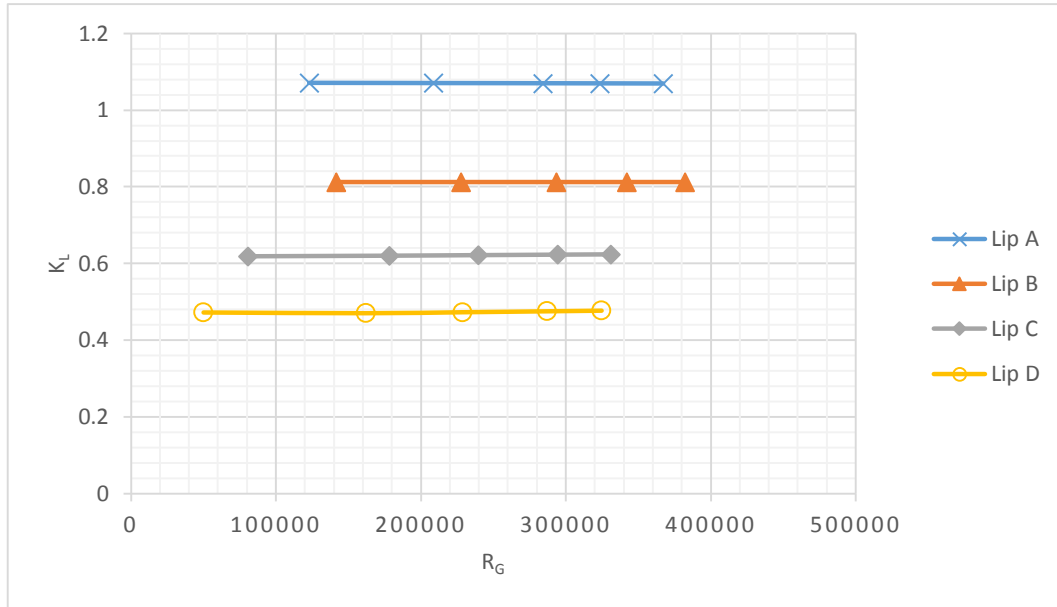


Figure 3.14 Downpull coefficient—Reynolds number relationship,  $y=0.2$   
(Computational)

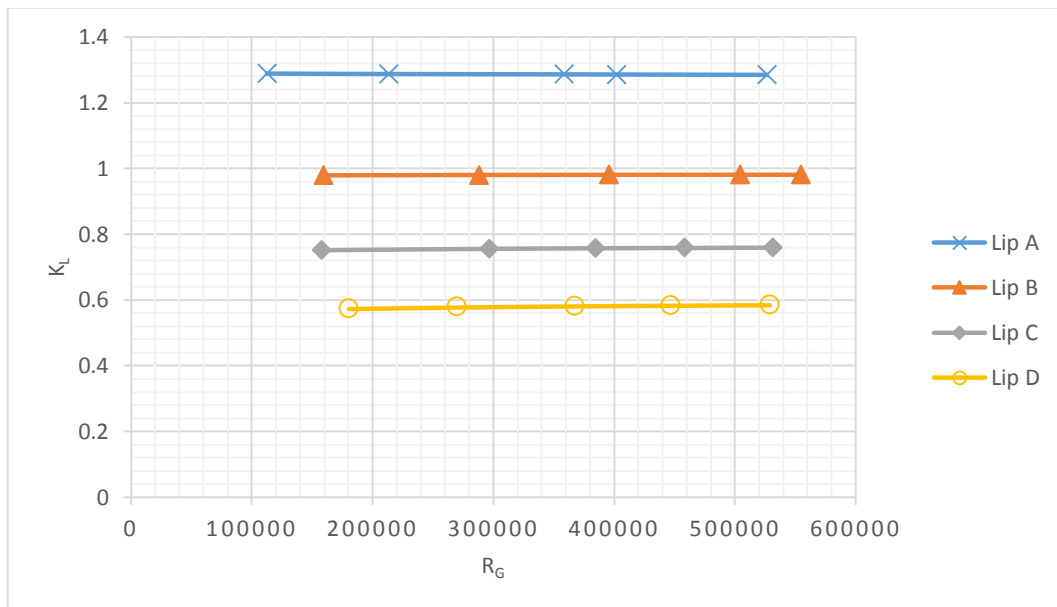


Figure 3.15 Downpull coefficient—Reynolds number relationship,  $y=0.4$   
(Computational)

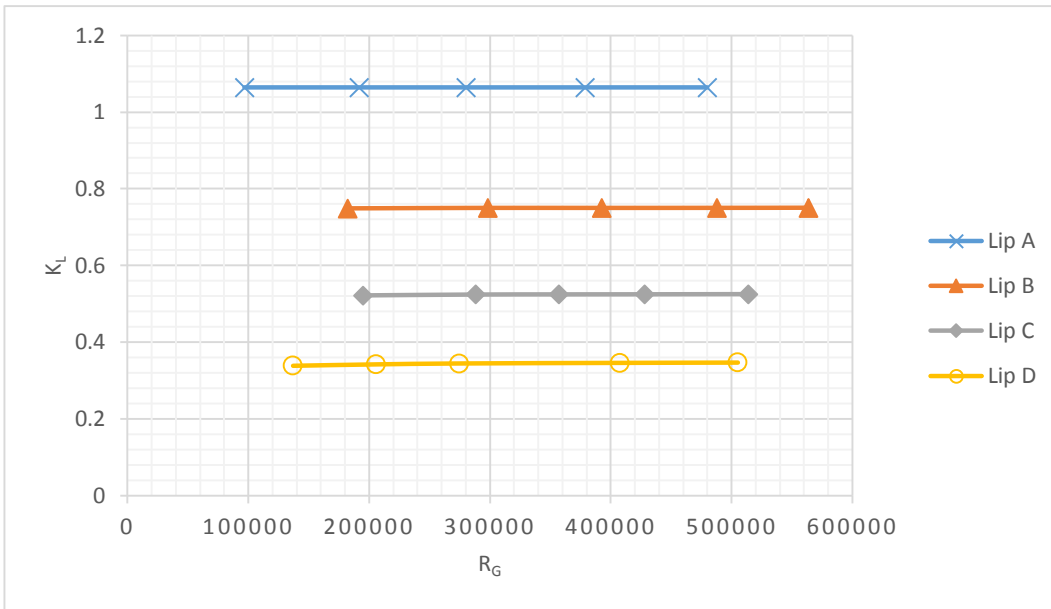


Figure 3.16 Downpull coefficient—Reynolds number relationship,  $y=0.6$  (Computational)

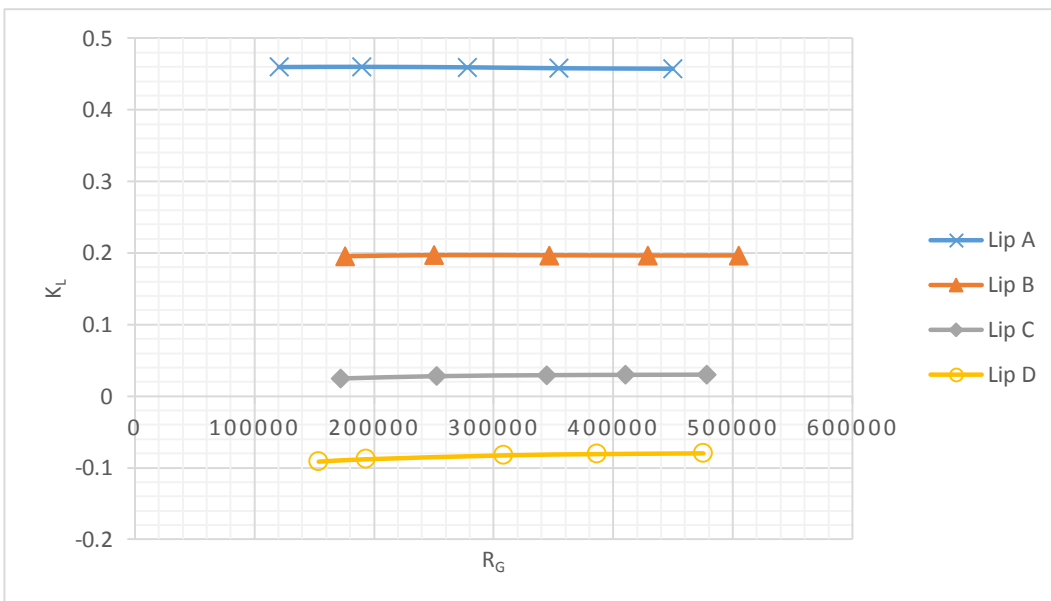


Figure 3.17 Downpull coefficient—Reynolds number relationship,  $y=0.8$  (Computational)

### **3.6 Comparison of Selected Flow Properties**

Three different properties, which are velocity magnitude, streamlines and turbulent kinetic energy are selected to be graphically presented and compared for selected cases. Velocity profiles under the gate lip section are also given. The case selection is made to show variations in critical models.

First, to investigate the effects of gate opening, lip angle is kept constant and the gate opening is changed for a maximum discharge that can pass for that gate opening.  $\theta=26.5^\circ$  is selected to be the lip angle to be kept constant. Three gate openings are selected for a constant lip angle, which are  $y=0.1$ ,  $y=0.5$  and  $y=0.9$ .

Then, lip angle is changed for a fixed gate opening with a maximum discharge to show how the lip angle influences the solution. 40% gate opening ( $y=0.4$ ) is selected to be kept constant and the solutions are compared for four different gate lips. Note that 40% is the gate opening where  $K_L$  value reaches its maximum value where sudden pressure changes are observable.

Finally, lip angle and gate opening is kept constant while changing the discharge to demonstrate the effects of discharge on a typical model.  $\theta=51.6^\circ$  and  $y=0.2$  are selected to be fixed while changing the discharge value.

#### **3.6.1 Effect of Gate Opening**

Changes in the flow for three different gate openings, which are  $y=0.1$ ,  $y=0.5$  and  $y=0.9$  are investigated. Figure 3.18 shows the velocity magnitude at three different gate openings, namely  $y=0.1$ ,  $y=0.5$  and  $y=0.9$ . It is seen that flow is accelerating under the gate section where the maximum velocity magnitude observed at that section is getting smaller as the gate opening increases. Most crucial values are occurring at the gate opening of 10% where the maximum velocity magnitude is around 4.89 m/s. Velocity magnitudes remain to be larger close to the bottom of the gate at the downstream of the gate section.

Velocity profiles under the gate lip sections are given in Figure 3.19. It is seen that the velocity under the gate increases as the gate opening decreases. At 90% gate opening there is a relatively uniform velocity distribution; as the gate opening decreases to 50% and 10% a sharp velocity gradient is observed close to the gate lip where the maximum velocity within the cross section is observed. Recirculation regions form at the downstream of the gates where low values of velocity magnitudes are observed. These recirculation bubbles can also be identified from the streamline patterns shown in Figure 3.20. As the gate opening increases the size of the recirculation bubble at the downstream of the gate increases. For the three gate openings investigated the lengths of the recirculation bubbles are 2.67 m, 2.78 m and 1.28 m respectively for increasing gate opening. In the 10% and 50% gate openings a small second recirculation bubble forms at the upstream of the gate. This formation is not visible at 90% gate opening. Turbulent kinetic energy contours on the flow domain for the three gate openings investigated is given in Figure 3.21. At all gate openings turbulent kinetic energy values are amplified along the shear layers which separates the fast moving flow close to the bottom of the duct from the low velocity flow inside the recirculating region. As the gate opening decreases the level of amplification in the turbulent kinetic energy values increase. The maximum turbulent kinetic energy value observed in 10% gate opening is 64% and 513% larger than the corresponding values observed in 50% and 90% gate openings. One interesting observation here is that the decay of energy takes places in approximately 3 meters for 10% gate opening (Fig. 3.21a) whereas the decay length is larger than 4.5 meters in %50 gate opening (Fig. 3.21b).

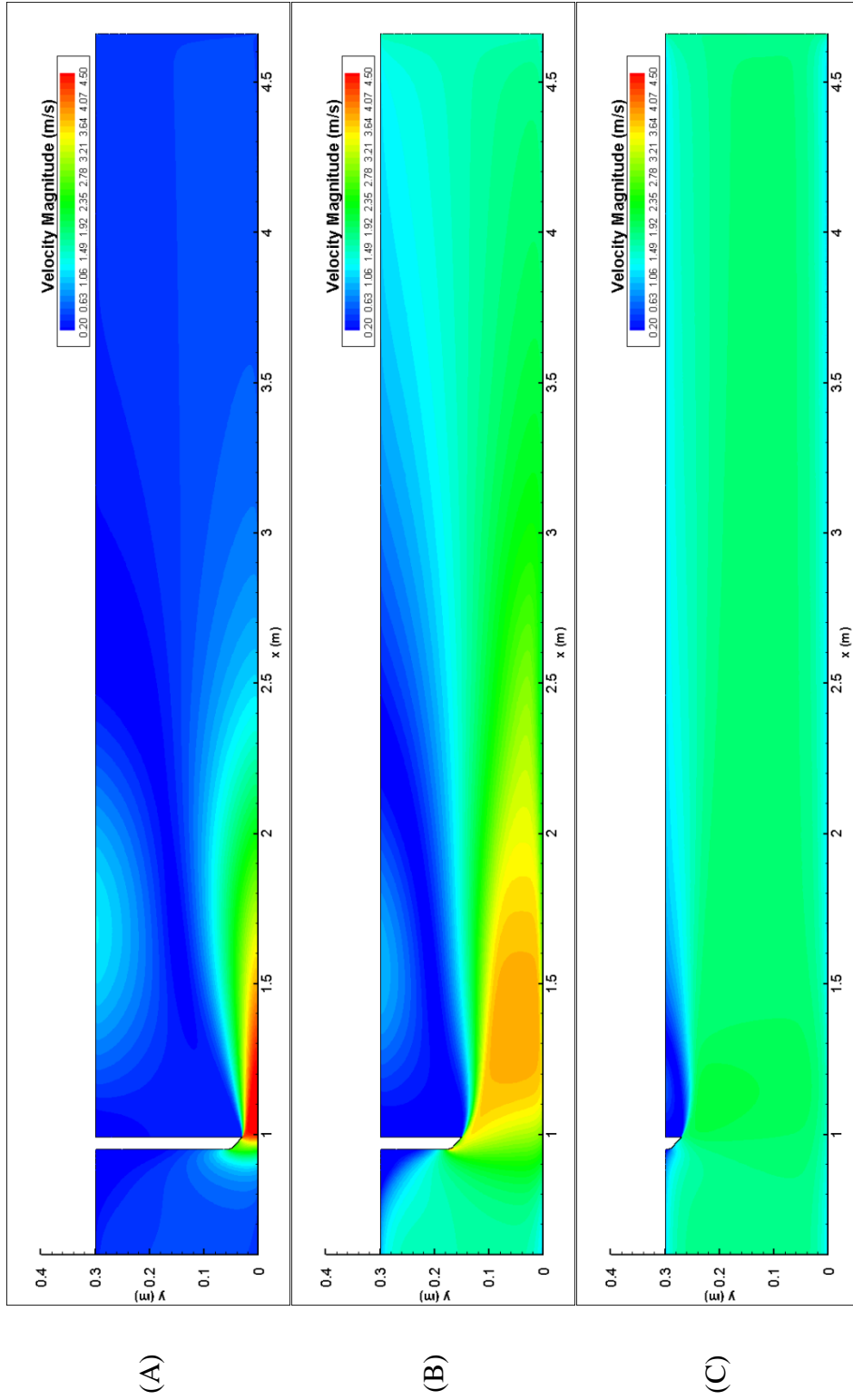


Figure 3.18 Velocity magnitude distribution for (A)  $\theta=26.5^\circ$ ,  $y=0.1$ ,  $Q=0.0295 \text{ m}^3/\text{s}$ , (B)  $\theta=26.5^\circ$ ,  $y=0.5$ ,  $Q=0.1107 \text{ m}^3/\text{s}$ , (C)  $\theta=26.5^\circ$ ,  $y=0.9$ ,  $Q=0.1216 \text{ m}^3/\text{s}$

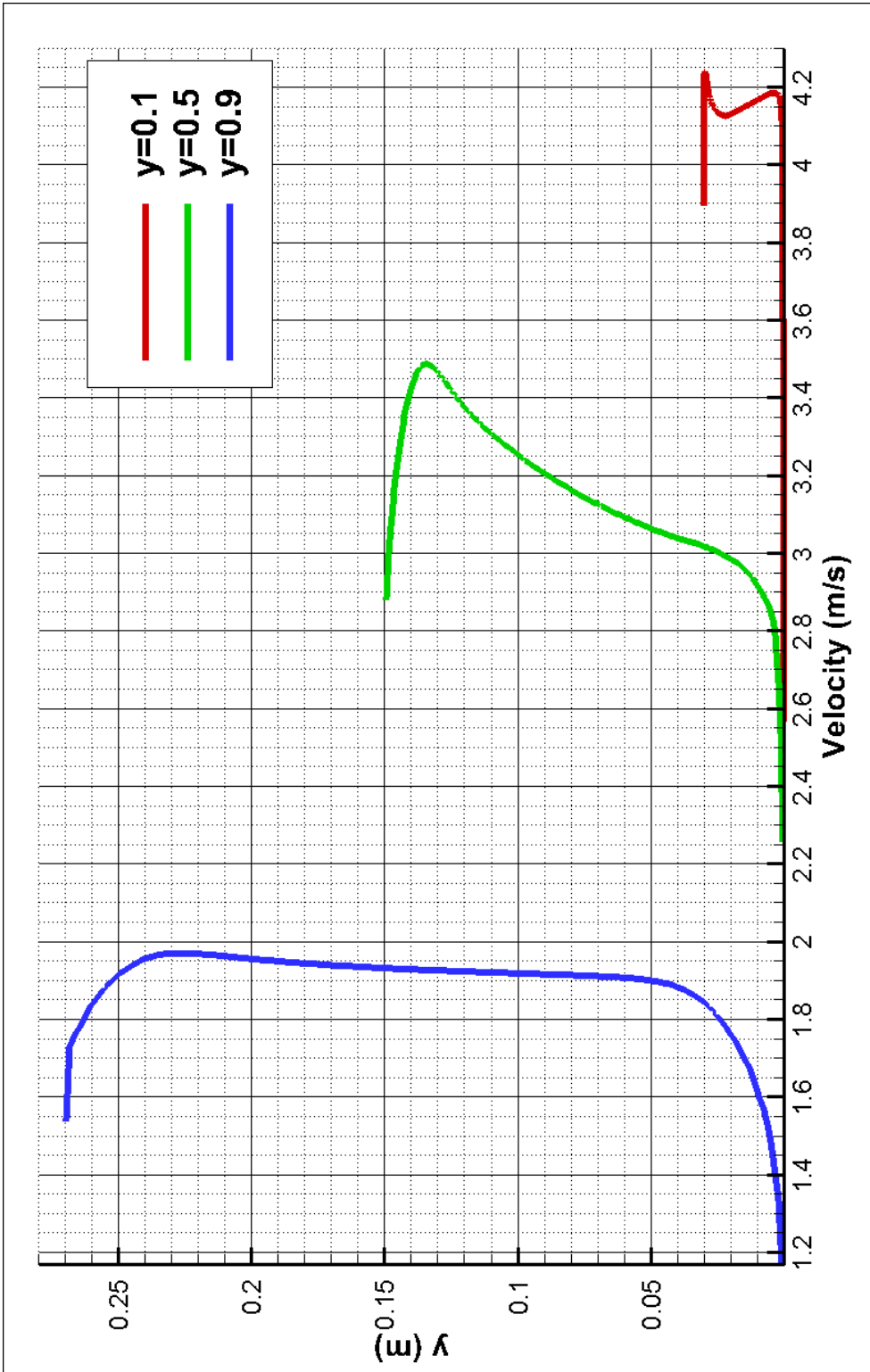


Figure 3.19 Velocity profiles under the gate section for  $y=0.1$ ,  $y=0.5$  and  $y=0.9$

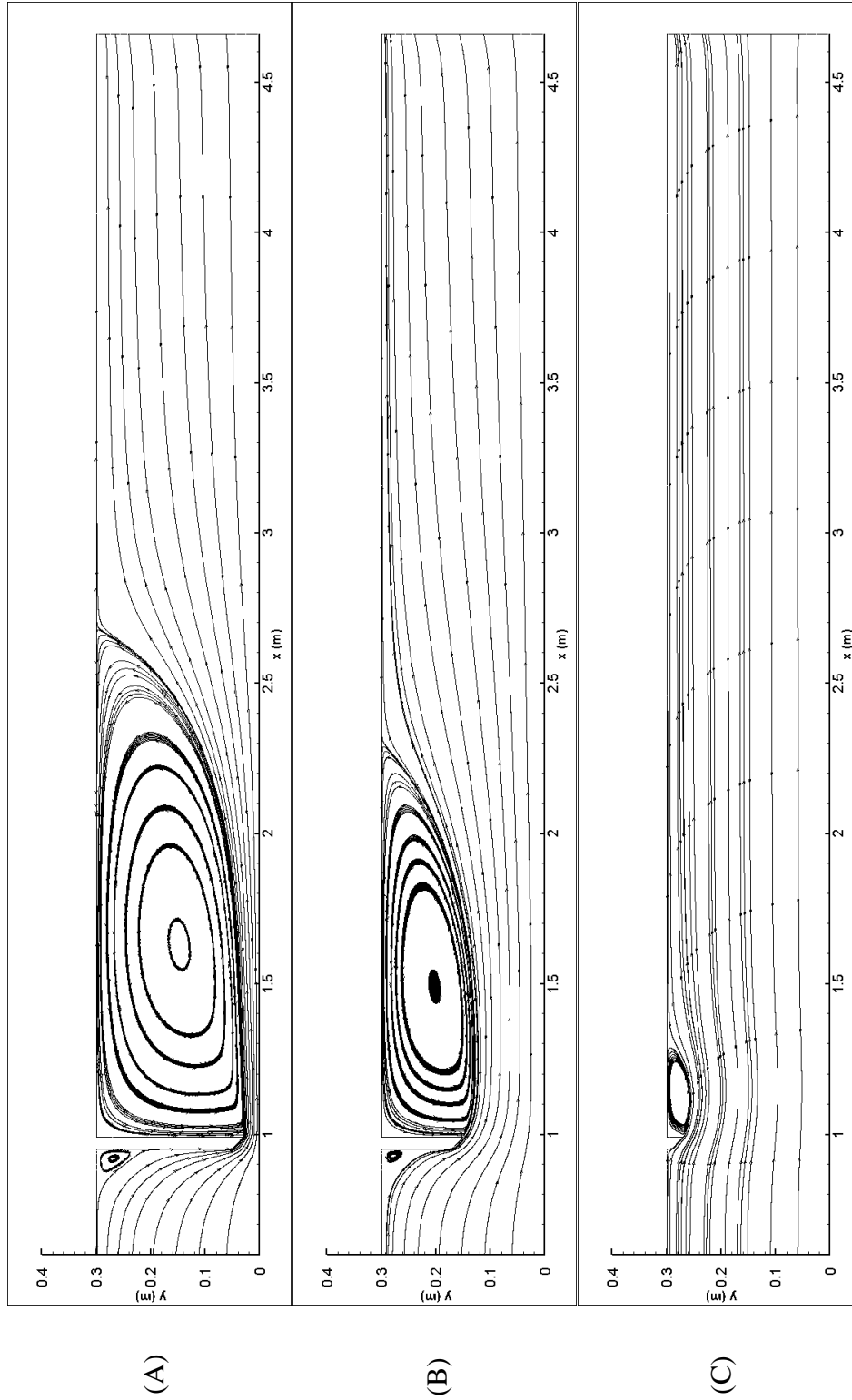


Figure 3.20 Streamlines for (A)  $\theta=26.5^\circ$ ,  $y=0.1$ ,  $Q=0.0295 \text{ m}^3/\text{s}$ , (B)  $\theta=26.5^\circ$ ,  $y=0.5$ ,  $Q=0.1107 \text{ m}^3/\text{s}$ , (C)  $\theta=26.5^\circ$ ,  $y=0.9$ ,  $Q=0.1216 \text{ m}^3/\text{s}$

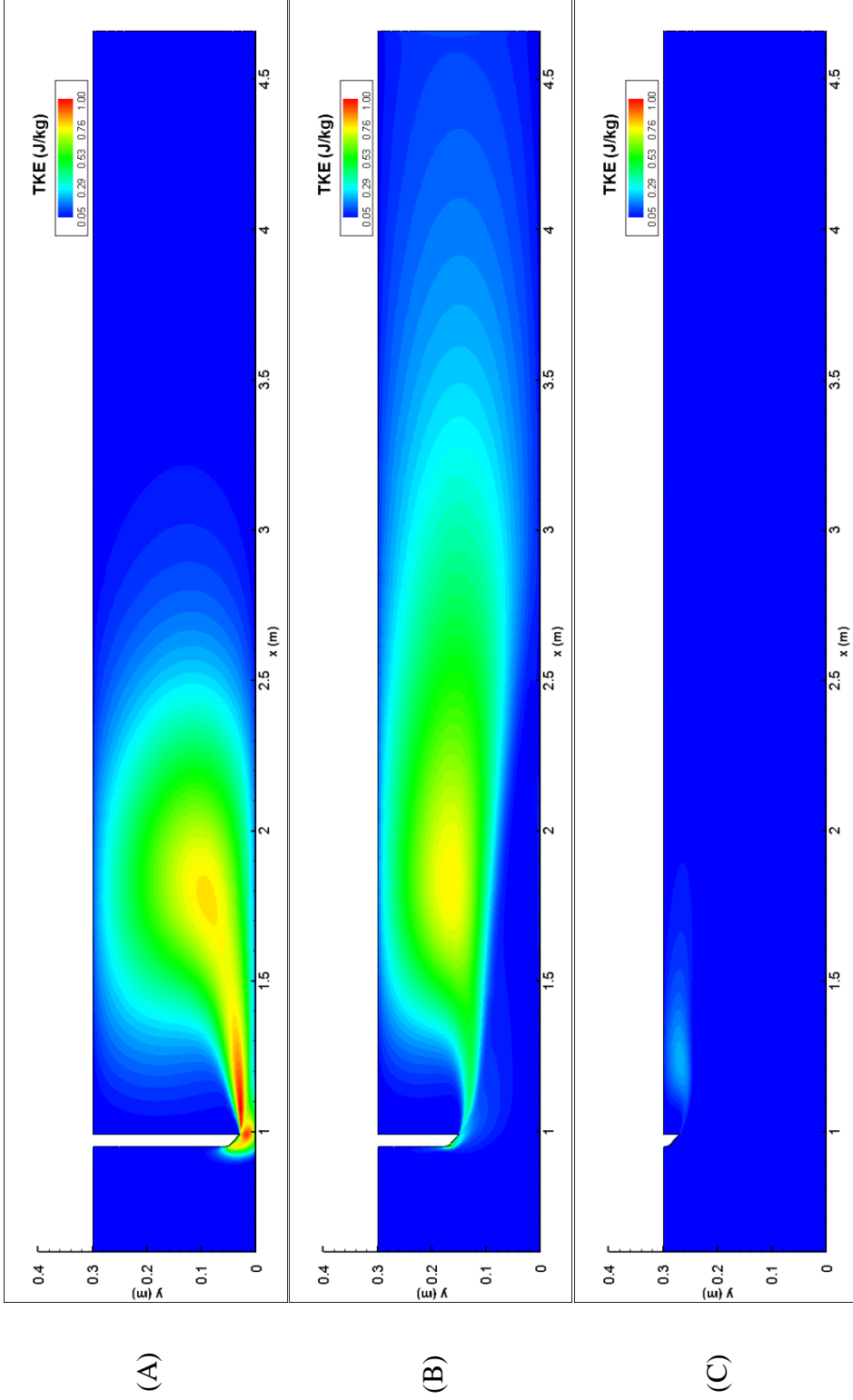


Figure 3.21 Turbulent Kinetic Energy for (A)  $\theta=26.5^\circ$ ,  $y=0.1$ ,  $Q=0.0295 \text{ m}^3/\text{s}$ , (B)  $\theta=26.5^\circ$ ,  $y=0.5$ ,  $Q=0.1216 \text{ m}^3/\text{s}$ , (C)  $\theta=26.5^\circ$ ,  $y=0.9$ ,  $Q=0.1107 \text{ m}^3/\text{s}$

### 3.6.2 Effect of Lip Angle

Changes in the flow for four different lip angles, which are  $\theta=26.5^\circ$ ,  $\theta=36.7^\circ$ ,  $\theta=44.7^\circ$  and  $\theta=51.6^\circ$ , are investigated. Velocity magnitude contours around the gate for the different lip angles at 40% gate opening are given in Figure 3.22. Velocity magnitudes are amplified beneath the gate for all the lip angles. However this amplification is largest at  $\theta=51.6^\circ$  and smallest at  $\theta=26.5^\circ$ . Keeping in mind that discharge values are slightly different for the four different gate lip angles and is largest for the lip angle of  $\theta=36.7^\circ$  one can say that the amplification in the velocity magnitude increases as the gate lip angle increases. Figure 3.23 shows the velocity profiles under tip of the gate lip sections. It is seen that for large lip angles ( $\theta \geq 44.7^\circ$ ), the velocity reaches its maximum value at a very close distance to the gate lip. Streamline patterns for the four lip angles investigated is given in Figure 3.24. For all the lip angles two recirculation regions one at the upstream and one at the downstream of the gate are present. As the lip angle increases the length of the downstream recirculation region slightly increases. Figure 3.25 shows the turbulent kinetic energy contours around the gate for the four different lip angles investigated. It can be seen from this figure that as the gate lip angle increases the level of turbulence at the downstream of the gate increases.

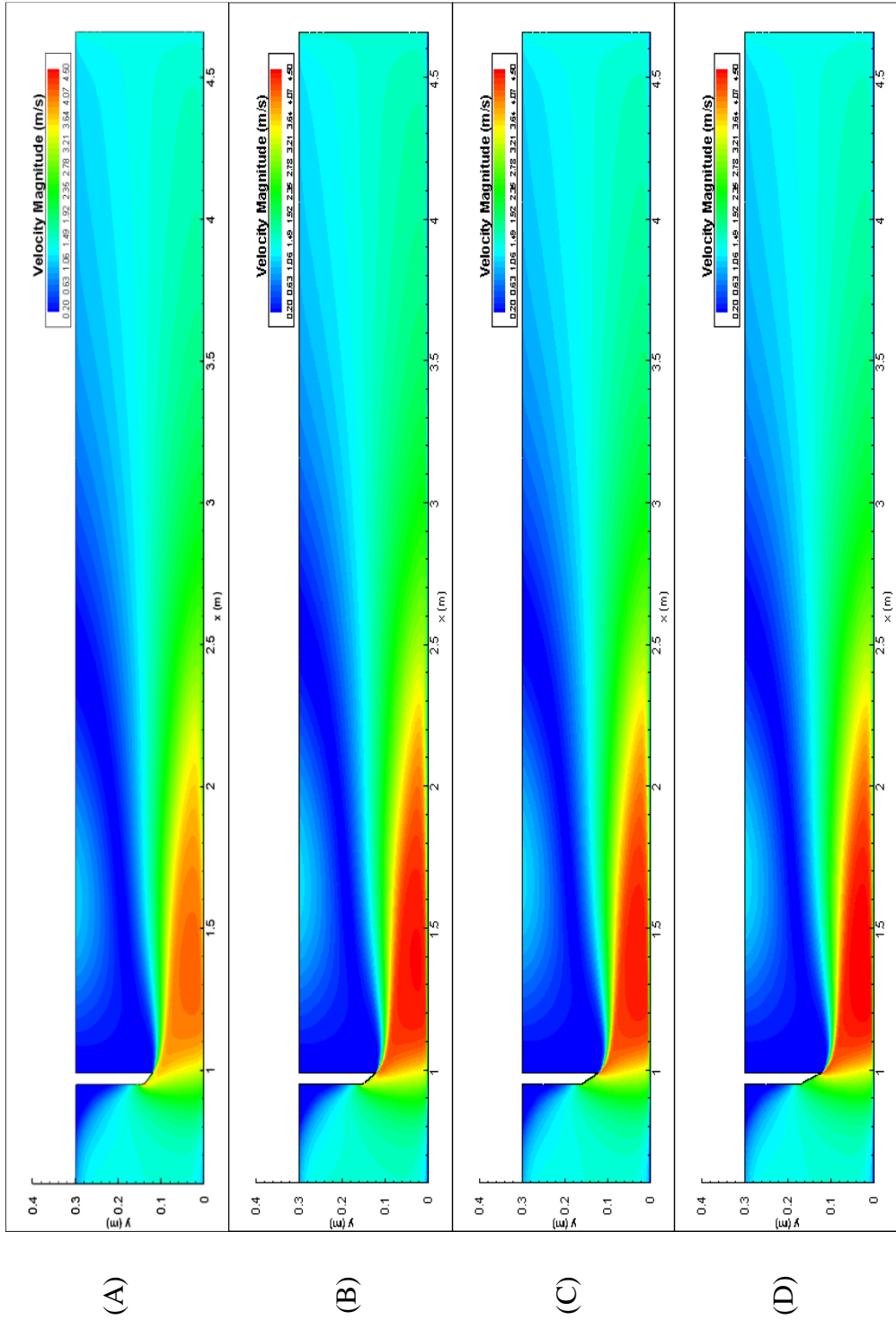


Figure 3.22 Velocity magnitude distribution for (A)  $\theta=26.5^\circ$ ,  $y=0.4$ ,  $Q=0.0947 \text{ m}^3/\text{s}$ , (B)  $\theta=36.7^\circ$ ,  $y=0.4$ ,  $Q=0.0997 \text{ m}^3/\text{s}$ , (C)  $\theta=44.7^\circ$ ,  $y=0.4$ ,  $Q=0.0955 \text{ m}^3/\text{s}$ , (D)  $\theta=51.6^\circ$ ,  $y=0.4$ ,  $Q=0.0953 \text{ m}^3/\text{s}$

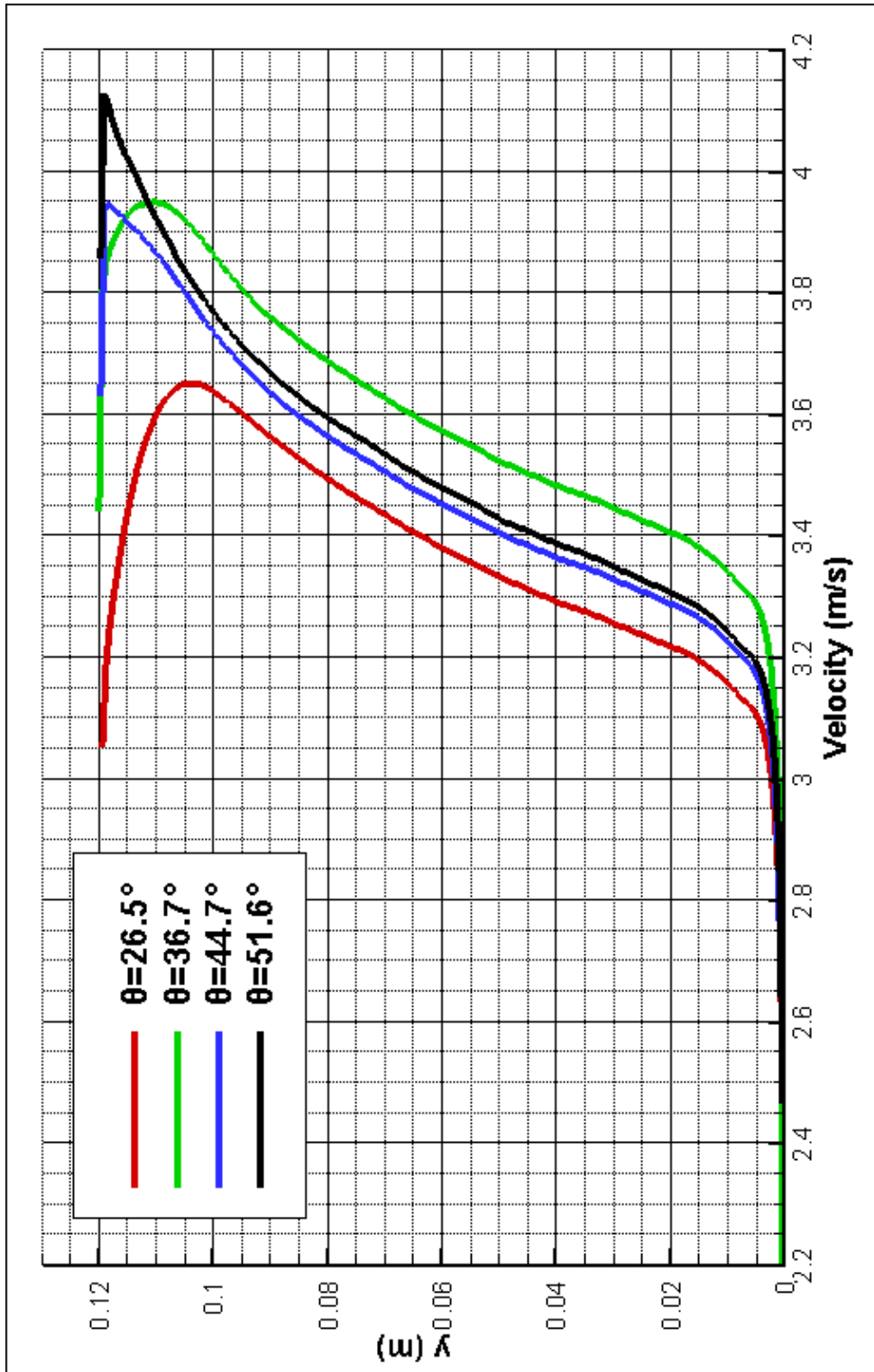


Figure 3.23 Velocity profiles under the gate section for  $\theta=26.5^\circ$ ,  $\theta=36.7^\circ$ ,  $\theta=44.7^\circ$  and  $\theta=51.6^\circ$

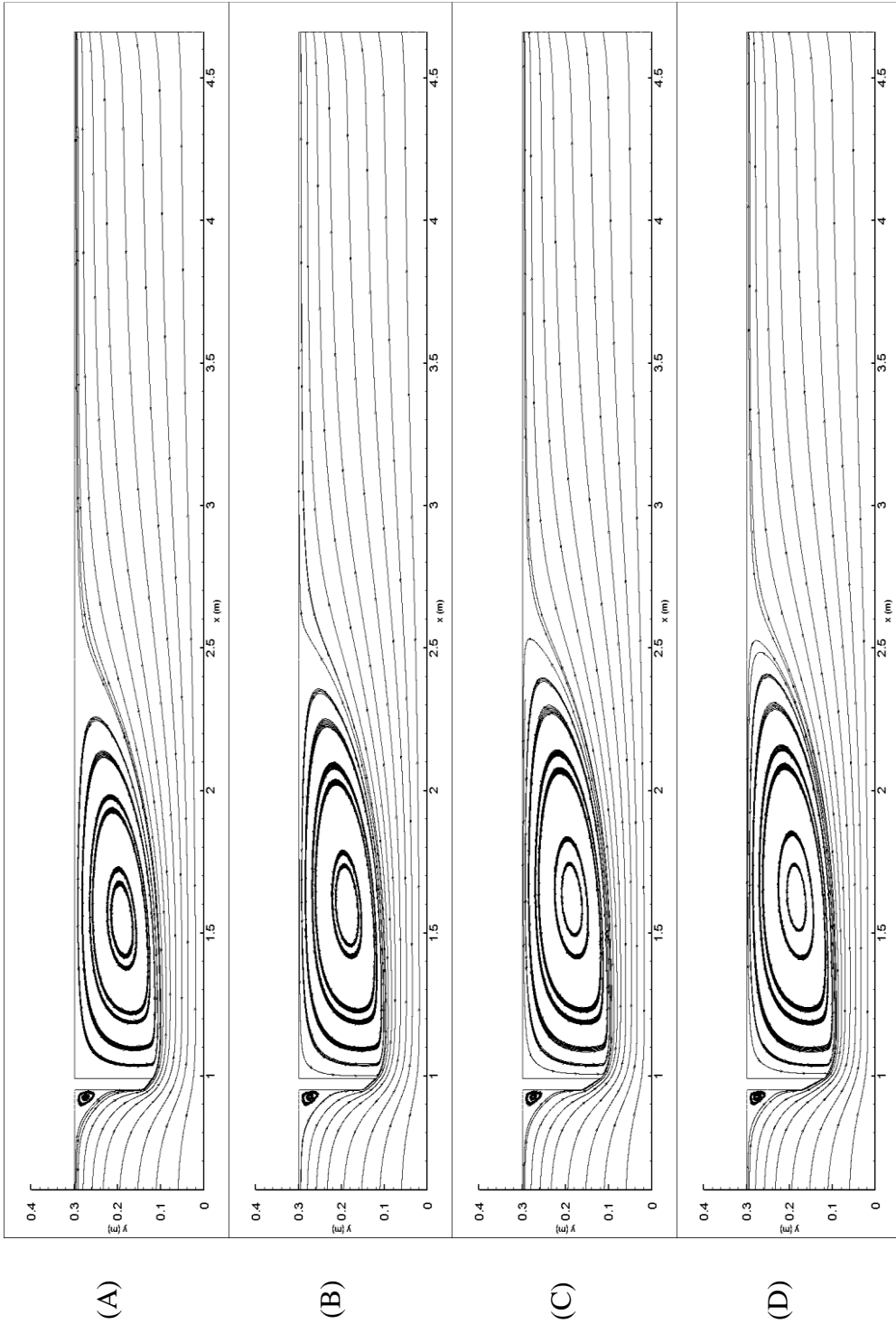


Figure 3.24 Streamlines for (A)  $\theta=26.5^\circ$ ,  $y=0.4$ ,  $Q=0.0947 \text{ m}^3/\text{s}$ , (B)  $\theta=36.7^\circ$ ,  $y=0.4$ ,  $Q=0.0997 \text{ m}^3/\text{s}$ , (C)  $\theta=44.7^\circ$ ,  $y=0.4$ ,  $Q=0.0955 \text{ m}^3/\text{s}$ , (D)  $\theta=51.6^\circ$ ,  $y=0.4$ ,  $Q=0.0953 \text{ m}^3/\text{s}$

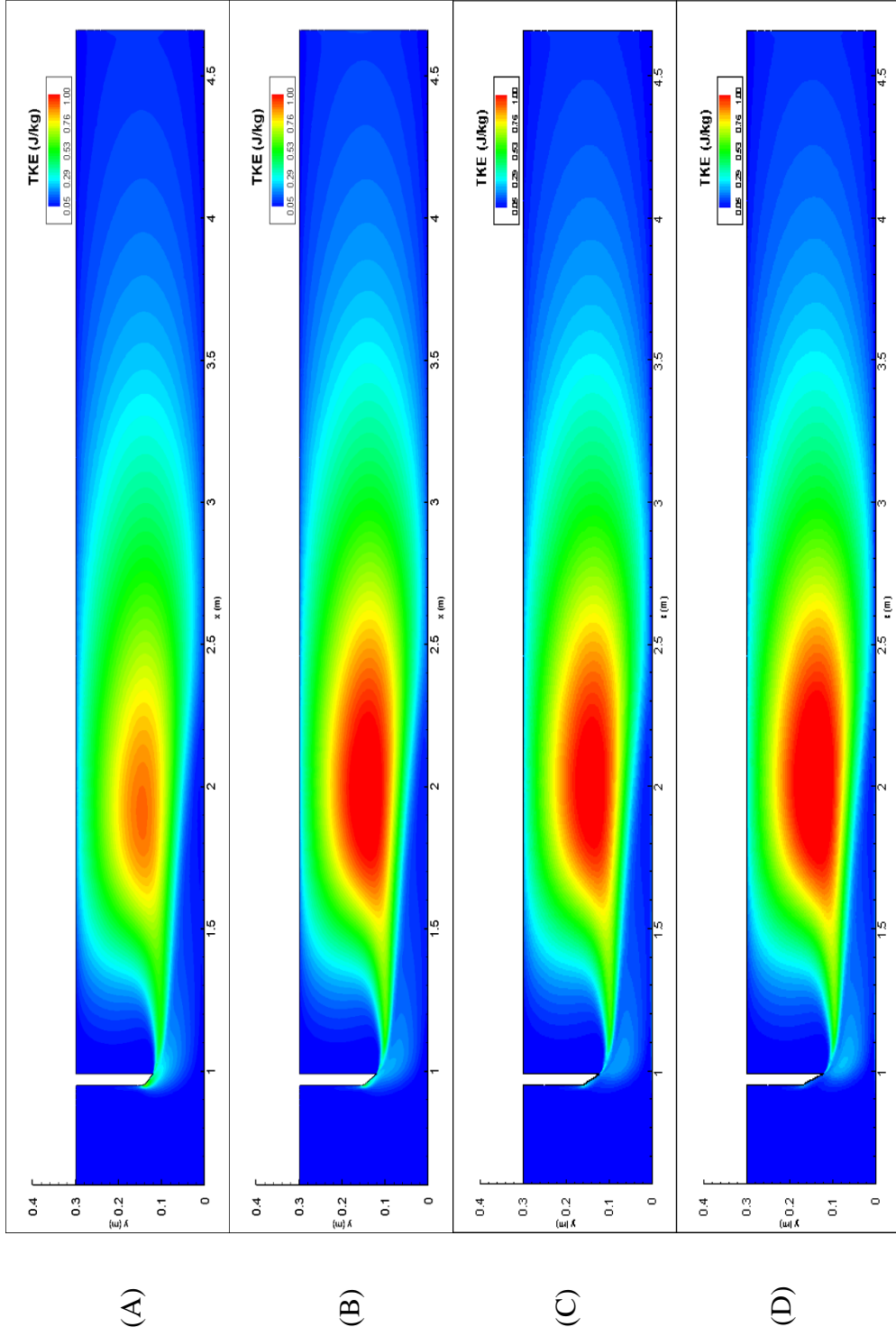


Figure 3.25 Turbulent Kinetic Energy for (A)  $\theta=26.5^\circ$ ,  $y=0.4$ ,  $Q=0.0947 \text{ m}^3/\text{s}$ , (B)  $\theta=36.7^\circ$ ,  $y=0.4$ ,  $Q=0.0997 \text{ m}^3/\text{s}$ , (C)  $\theta=44.7^\circ$ ,  $y=0.4$ ,  $Q=0.0955 \text{ m}^3/\text{s}$ , (D)  $\theta=51.6^\circ$ ,  $y=0.4$ ,  $Q=0.0953 \text{ m}^3/\text{s}$

### 3.6.3 Effect of Discharge

The velocity magnitude distributions, velocity profiles, streamlines and turbulent kinetic energy distributions for three different discharge values, which are  $Q=0.0075 \text{ m}^3/\text{s}$ ,  $Q=0.0343 \text{ m}^3/\text{s}$  and  $Q=0.0487 \text{ m}^3/\text{s}$ , are compared in Figures 3.26, 3.27, 3.28 and 3.29 respectively. As expected, once the discharge is increased, larger velocity magnitudes are observed beneath the gate (Figure 3.26 and Figure 3.27). As the discharge increases the peak velocity observed just beneath the gate considerably increases. Downstream recirculation regions have almost the same length for all of the discharges investigated (Figure 3.28), whereas the turbulent kinetic energy values considerably increases with the increase in discharge (Figure 3.29).

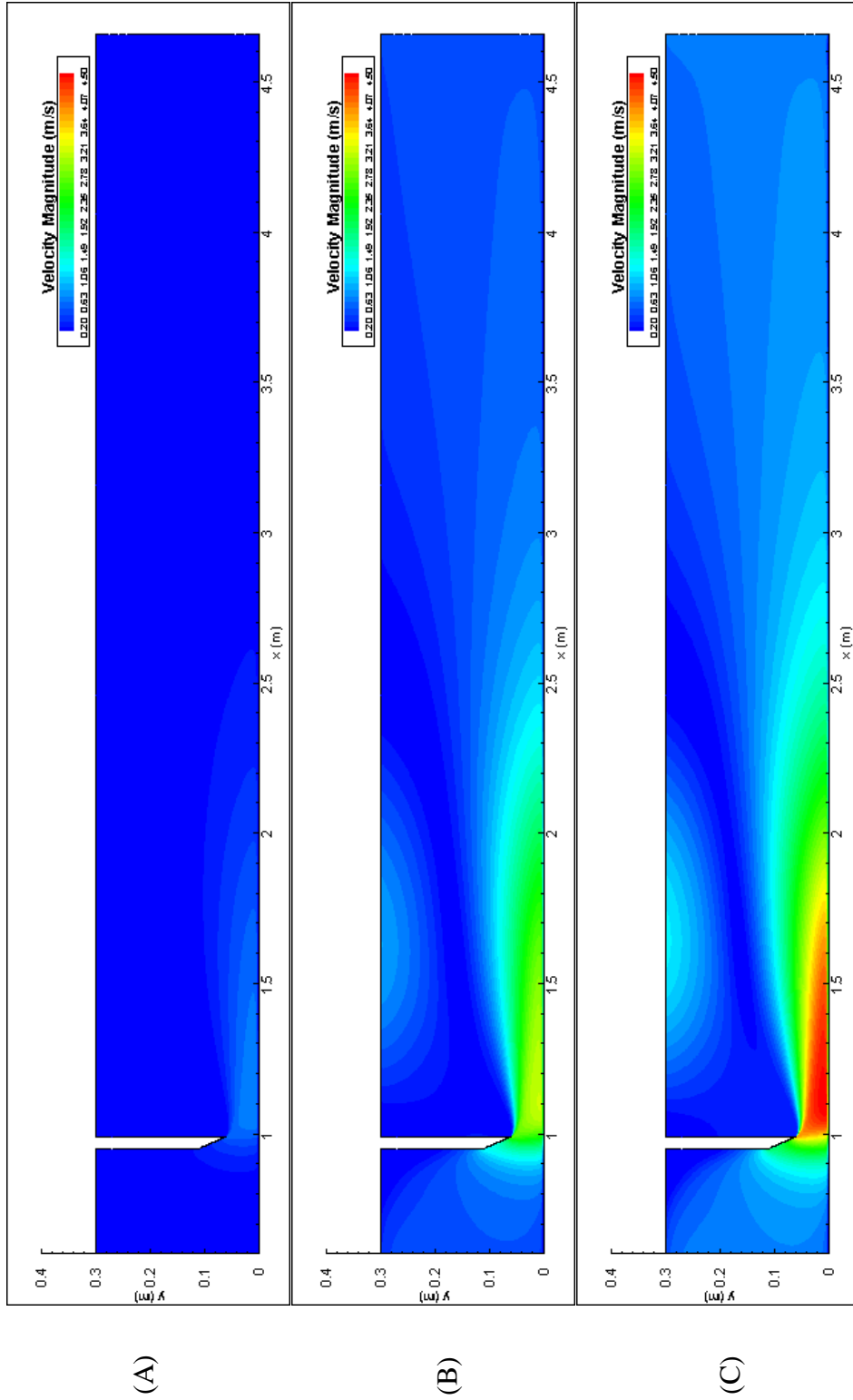


Figure 3.26 Velocity magnitude distribution for (A)  $\theta=51.6^\circ$ ,  $y=0.2$ ,  $Q=0.0075 \text{ m}^3/\text{s}$ , (B)  $\theta=51.6^\circ$ ,  $y=0.2$ ,  $Q=0.0343 \text{ m}^3/\text{s}$ , (C)  $\theta=51.6^\circ$ ,  $y=0.2$ ,  $Q=0.0487 \text{ m}^3/\text{s}$

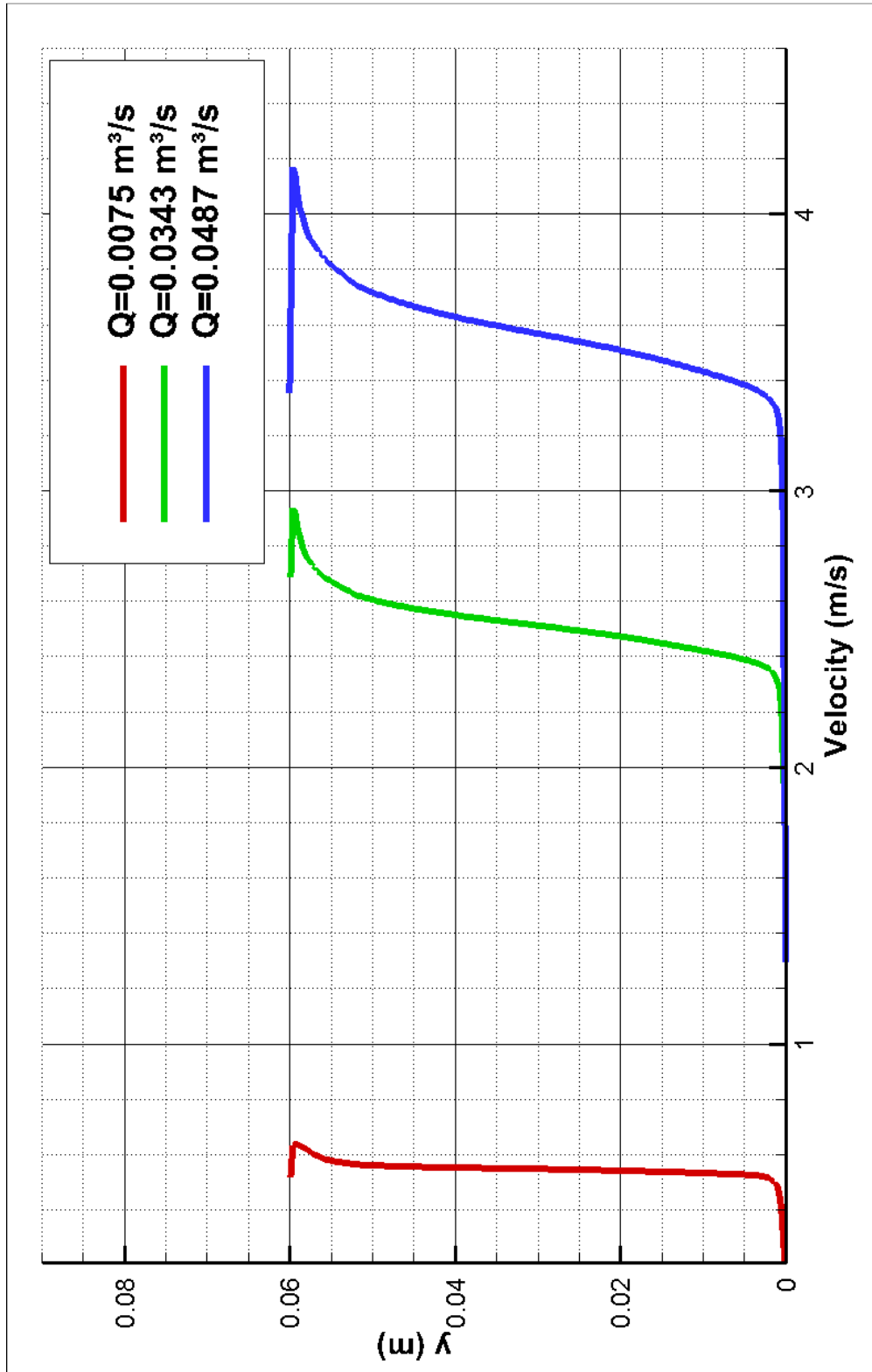


Figure 3.27 Velocity profiles under the gate section for  $Q=0.0075 \text{ m}^3/\text{s}$ ,  $Q=0.0343 \text{ m}^3/\text{s}$  and  $Q=0.0487 \text{ m}^3/\text{s}$

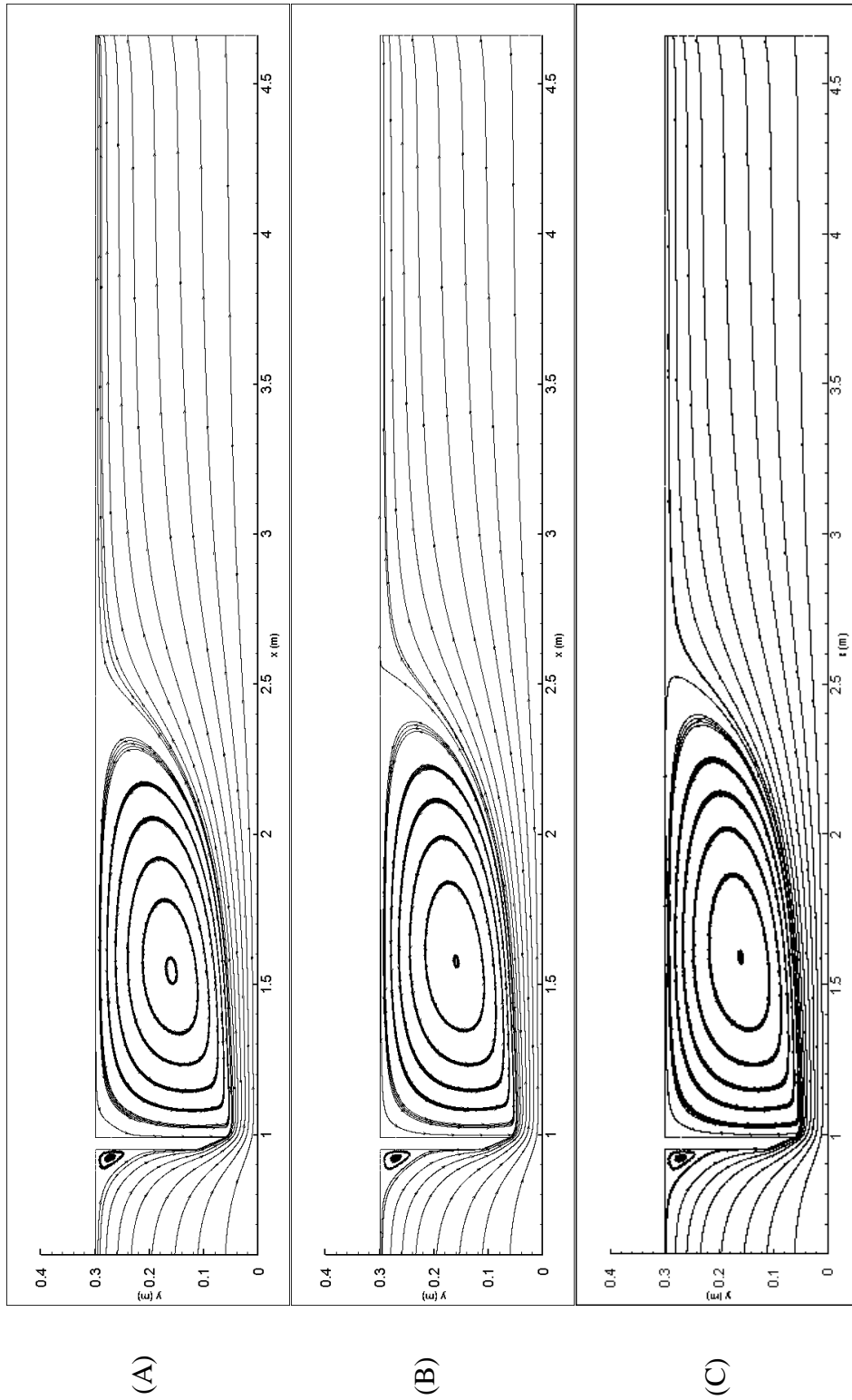


Figure 3.28 Streamlines for (A)  $\theta=51.6^\circ$ ,  $y=0.2$ ,  $Q=0.0075 \text{ m}^3/\text{s}$ , (B)  $\theta=51.6^\circ$ ,  $y=0.2$ ,  $Q=0.0343 \text{ m}^3/\text{s}$ ,  
 (C)  $\theta=51.6^\circ$ ,  $y=0.2$ ,  $Q=0.0487 \text{ m}^3/\text{s}$

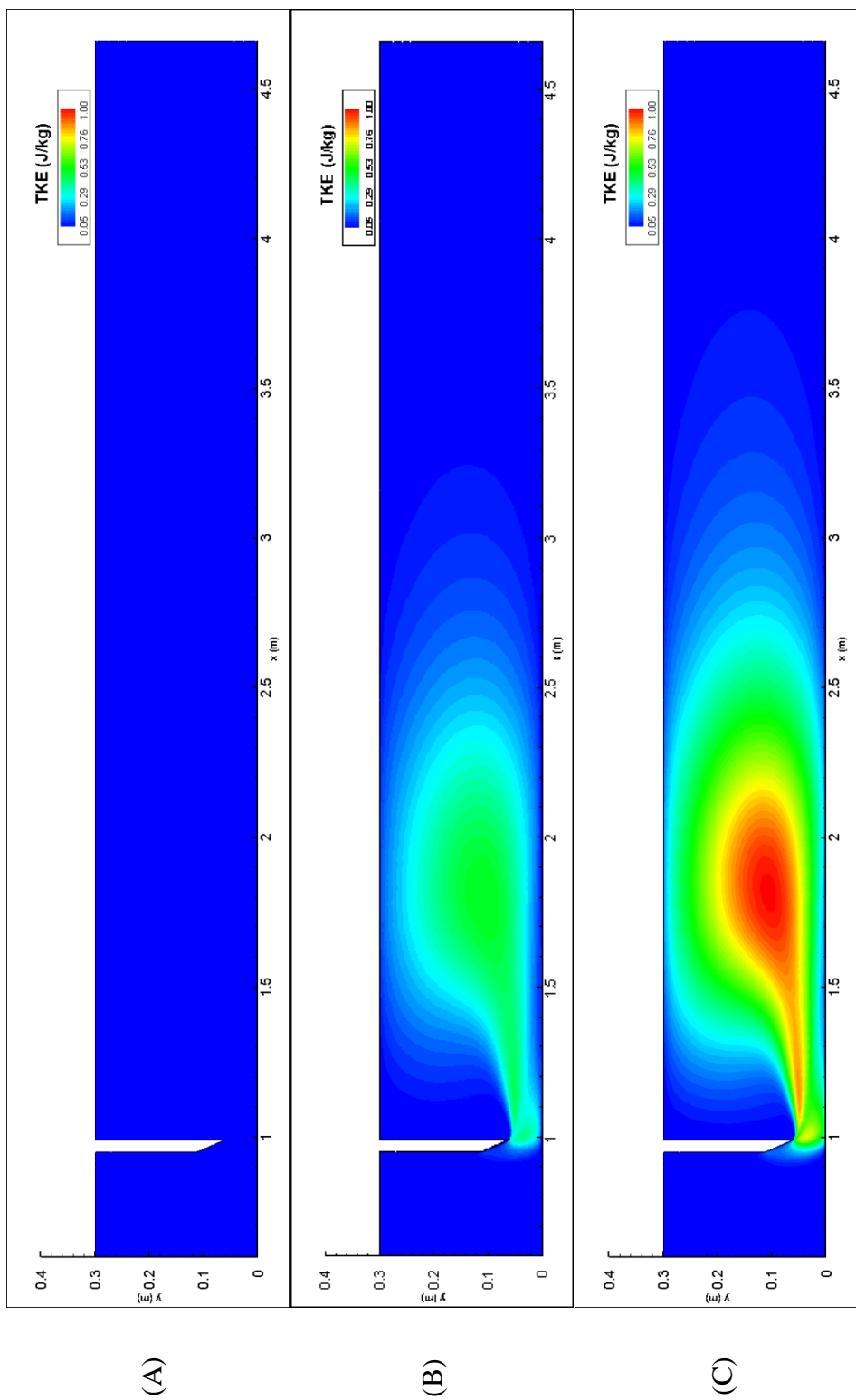


Figure 3.29 Turbulent Kinetic Energy for (A)  $\theta=51.6^\circ$ ,  $y=0.2$ ,  $Q=0.0075 \text{ m}^3/\text{s}$ , (B)  $\theta=51.6^\circ$ ,  $y=0.2$ ,  $Q=0.0343 \text{ m}^3/\text{s}$ , (C)  $\theta=51.6^\circ$ ,  $y=0.2$ ,  $Q=0.0487 \text{ m}^3/\text{s}$

### 3.7 Lip Downpull Coefficient as a Function of the Gate Opening and the Lip Angle

Figure 3.30 demonstrates downpull coefficient as a function of the gate lip angle and gate opening, which is based on experimental study of Aydin et al. (2003). The details of this study is given in Chapter 2.

Lip downpull coefficient,  $K_L$  is zero at each side of the Figure 3.30, where the gate is fully open ( $y=1$ ) and fully closed ( $y=0$ ). The reason for this is that at these two gate openings, the piezometric head acting on the gate lip is equal to the piezometric head of the gate section. It can be seen from the figure that the downpull coefficient is at its maximum around 30-40% gate openings. The downpull coefficient is increasing with the decreasing gate lip angle. Around 90% gate openings, the downpull coefficient is negative which indicates that the piezometric head on the gate lip is larger than the piezometric head at the gate section. In that case, an uplift occurs instead of a downpull.

As it is done in the experimental study,  $K_L$  is stated as a polynomial where  $y$  is the independent variable using data coming from computational results. The  $K_L$  function will also be presented as two parts, the same as the experimental study.

For  $0 < y < 0.8$

$$K_L = (11 - 0.155320 + 0.00024897)y + (-12.429 - 0.0929610 + 0.00436190^2)y^2 + (-13.521 + 1.16270 - 0.0175380^2)y^3 + (17.107 - 1.05510 + 0.014670^2)y^4 \quad (3.1.a)$$

For  $0.8 \leq y < 1$

$$K_L = (317.08 - 2.122030 - 0.0305470^2) + (-1485.1 + 4.65050 + 0.222510^2)y + (2600.9 + 2.710 - 0.548360^2)y^2 + (-2004.1 - 12.1280 + 0.566830^2)y^3 + (570.65 + 6.930720 - 0.21095)y^4 \quad (3.1.b)$$

Because of the non-linearity of the  $y$ - $K_L$  curve, it is hard to obtain a generalized solution. Coefficients of equation (2.5) are taken as initial guesses for the optimization of the computational data. It should be noted that there is more than one solution for each of the mentioned ranges, namely,  $0 < y < 0.8$  and  $0.8 \leq y < 1$ . Regardless of any similarities between coefficients of equation (3.1) and (2.5), the equations obtained from computational study give similar results to the experimental data.

Equation 3.1 is valid for  $26^\circ \leq \theta \leq 52^\circ$ . Equation 3.1 will give the lip downpull coefficient,  $K_L$ , for given  $y$  and  $\theta$ , and the downpull on the gate lip can be evaluated using this result.

Complete data set for the lip downpull coefficient,  $K_L$ , evaluated using computed data of this study are shown in Figure 3.30.

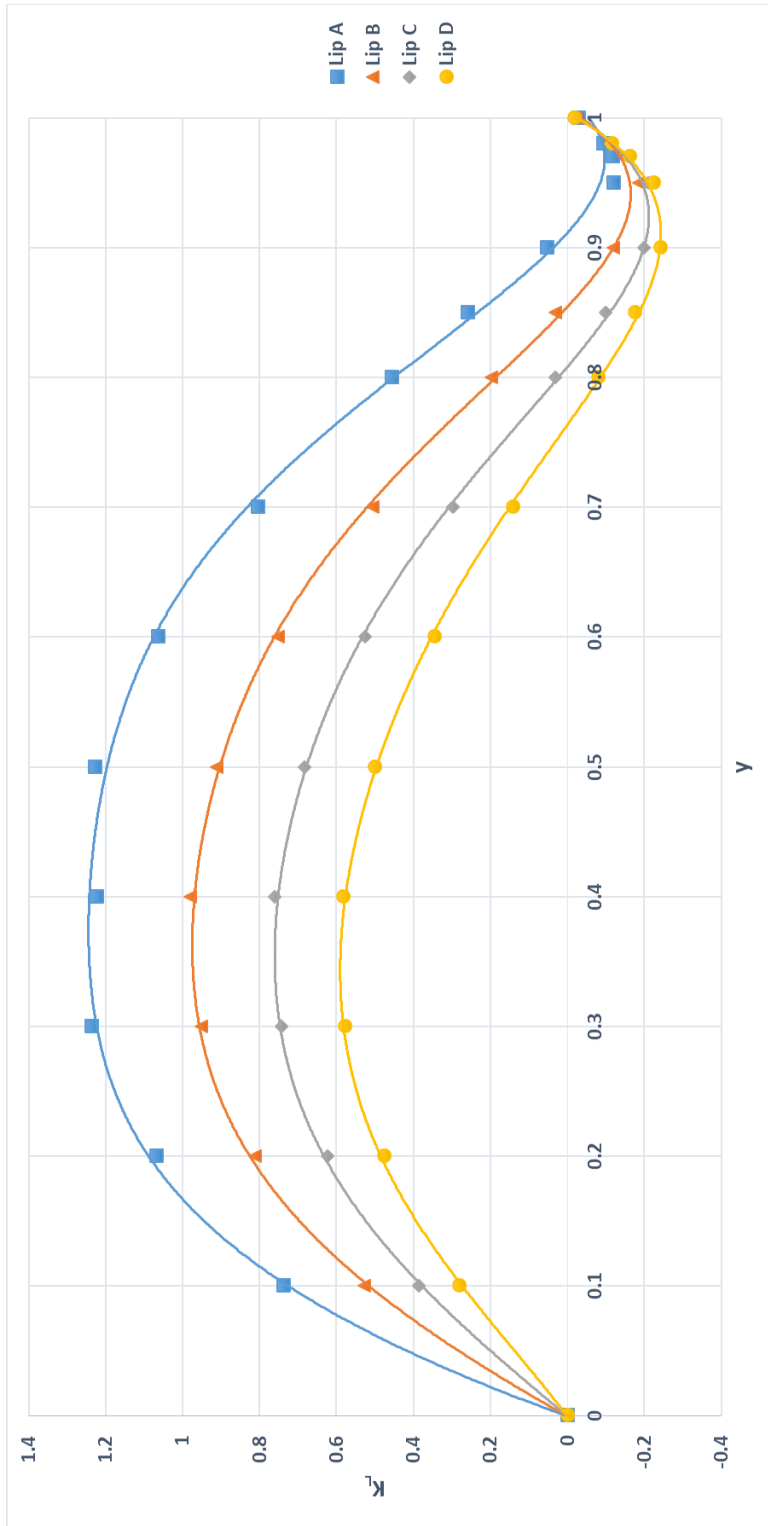


Figure 3.30 Downpull coefficient as a function of the gate lip angle and the gate opening (Computational)

### 3.8 Comparison of Experimental and Computational Values

Generally, two dimensional approach is an idealization to the three dimensional model. In 2D, for large Reynolds numbers, there is no turbulence due to absence of vortex tube stretching in the third dimension. This prevents taking the effects of secondary flows into account. These effects become more important for large openings, which have larger velocity magnitudes, hence larger Reynolds numbers.

As it is mentioned in Chapter 2, the experimental model had a gate chamber, which is absent for the computational model. For small gate openings, the momentum of the flow and the pressure difference leads the water to flow over the gate, through the gate chamber, causing leakage. Again, when the gate is fully closed, the experimental model might not be able to prevent leakage, both through gate chamber and beneath the gate.

In preceding sections, downpull coefficient  $K_L$  is presented as function of gate angle and the gate opening, both for experimental and computational. In Figure 3.31, the  $K_L$  values coming from the computational study is sketched together with Equation 2.5, to see the differences in dimensionless downpull coefficient,  $K_L$  between experimental and computational study.

Figure 3.31 shows that the computational  $K_L$  values are matching with the Equation 2.5 where  $y$  is less than 0.8, except for Lip A, which is  $26.5^\circ$ . The computational  $K_L$  values for Lip A between  $y=0.3$  and  $y=0.7$  seem to be a little off from the experimental results. However these values starts to get close to each other in range where  $y=0.8$  and  $y=0.9$ , where other values coming from other lip angles are apart from each other.

It is seen that after gate opening  $y=0.8$ , up to  $y=1.00$ , most computational  $K_L$  values seem to be far from experimental values. It should be noted here two gate openings ( $y=0.9333$  and  $y=0.9666$ ) used in the experiments conducted in hydraulic study, are not modeled in computational study. Instead, three different gate openings, which are  $y=0.95$ ,  $y=0.97$  and  $y=0.98$  are used, considering that the  $K_L$  values are more critical for gate openings close

to the fully opened gate. This may help to catch the behavior of the  $K_L$  near  $y=1.00$ . In Figure 3.31, between  $y=0.8$  and  $y=1.00$ , experimental  $K_L$  values are following a path away from the axis, compared to the computational values which remain close to the axis. Ultimately, both  $K_L$  values at  $y=1.00$  (where gate is fully opened) are zero or very close to zero, therefore, if a curve is formed from the values of the computational study, it would be more natural as it is following a smoother path (where there is no need for abrupt changes of  $K_L$  to reach 0 when  $y=1.00$ ) compared to the experimental study.

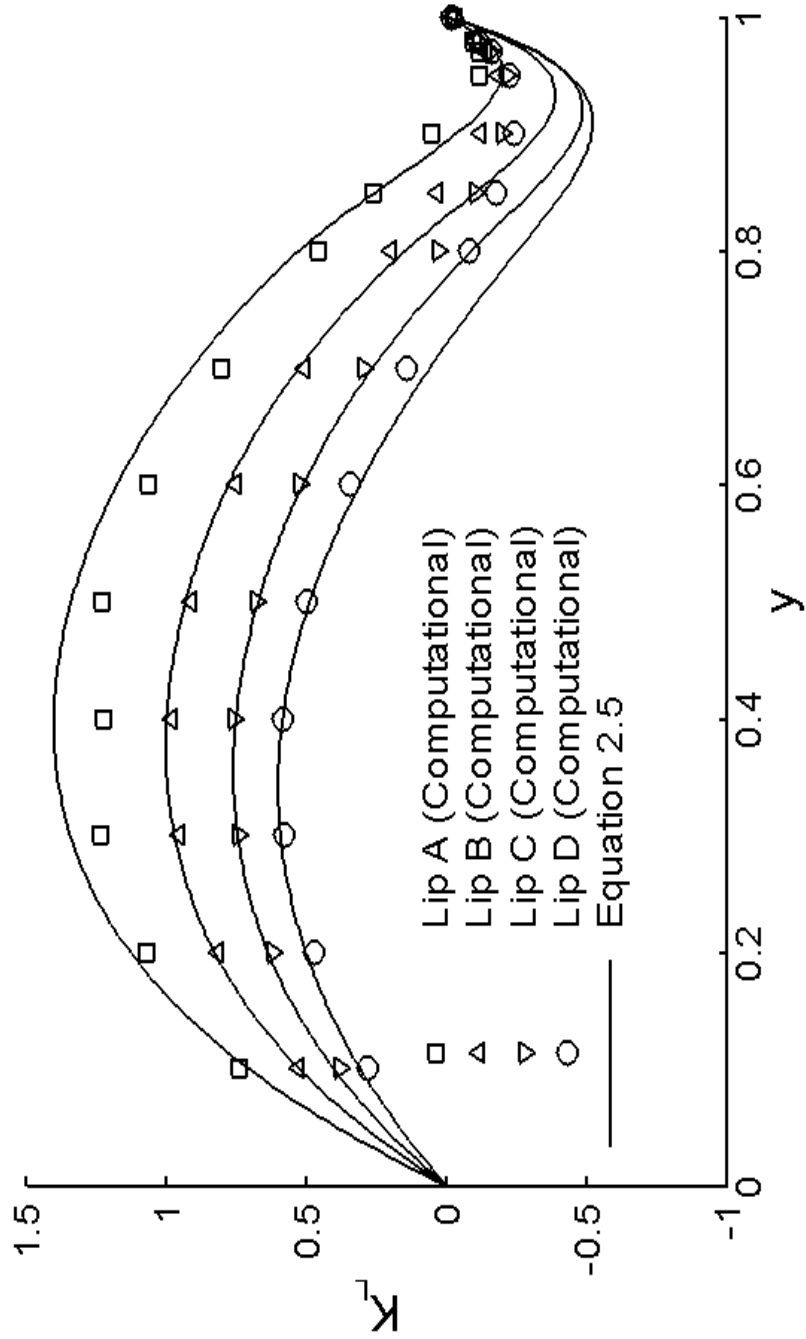


Figure 3.31 Downpull coefficient as a function of the gate lip angle and the gate opening  
(Computational and experimental comparison)

## CHAPTER 4

### CONCLUSION

In this thesis, hydrodynamic downpull force is studied computationally on the created models for variable gate openings and gate lip angles. Numerical models are generated to represent the flow in a penstock or a tunnel and effects of this flow on a tunnel gate are investigated.

It can be concluded that, for achieving the general accuracy of a CFD model, one should consider the properties geometry, meshing, turbulence model and boundary conditions. Domain size and the mesh generated for the simulations strongly affects the results.

- The inflow and outflow sections should be selected at a sufficiently large distance ( $10e_0$  and  $12e_0$  for upstream and downstream, respectively) from the gate section in order not to influence the results.
- Grid independence check should be made in order to decide on the mesh size to be used in the numerical study.
- Grid refinement should be made at locations where large gradients on flow quantities occur, or at locations where finer resolution is needed, i.e. because of flow separation.
- “Enhanced wall treatment” option in the turbulence model tab should be used for flows which are massively separated, as for these flows logarithmic velocity profile assumption is not valid.

The numerical simulations are efficient and less costly compared to the experimental methods. However, it would be very beneficial to have at least one validation case from a physical experiment. Yet, this thesis should be considered as a proof that CFD modelling is a substitution to physical models.

FLUENT can be used with confidence in calculating the hydrodynamic downpull coefficient  $K_L$  for vertical high head gates, provided that the domain size, mesh size and grid clustering is done correctly.

Steady, 2D flow assumptions are reasonable for the numerical simulations.

The range of applicability of findings of this study can be expanded by considering effects of a moving gate on the downpull. In addition, results coming out from this study can also be validated for a three dimensional model.

## REFERENCES

- Akoz, M. S., Kirkgoz, M. S., & Oner, A. A. (2009). Experimental and Numerical Modeling of a Sluice Gate Flow. *Journal of Hydraulic Research* 47:2, 167-176.
- Amorim, J. C., & Andrade, J. L. (1999). Numerical Analysis of the Hydraulic Downpull on Vertical Lift Gates. *Waterpower '99*, 1-9.
- Aydin, I. (2002). Air Demand Behind High Head Gates. *Journal of Hydraulic Research IAHR* 40:1, 83-93.
- Aydin, I., Dundar, O., & Telci, I. (2003). *Hydrodynamic Loads on Closing Hydraulic Gates (in Turkish)*. Ankara: METU.
- Aydin, I., Telci, I., & Dundar, O. (2006). Prediction of Downpull on Closing High Head Gates. *Journal of Hydraulic Research IAHR* 44:6, 822-831.
- Dargahi, B. (2010). Flow Characteristics of Bottom Outlets with Moving Gates. *Journal of Hydraulic Research* 48:4, 476-482.
- Erbisti, P. C. (2004). *Design of Hydraulic Gates*. Tokyo: A.A Balkema Publishers.
- Inc., A. (2011, November). ANSYS FLUENT User's Guide Release 14.0.
- Inc., F. (2007, May). GAMBIT 2.4 Documentation.
- Naudascher, E. (1986). Prediction and Control of Downpull on Tunnel Gates. *Journal of Hydraulic Engineering ASCE* 112:5, 392-416.
- Naudascher, E. (1991). *Hydrodynamic Forces*. Rotterdam: A.A. Balkema.

Naudascher, E., Kobus, H. E., & Rao, R. P. (1964). Hydrodynamic Analysis for High-head Leaf Gates. *Journal of the Hydraulics Division ASCE* 90:3, 155-192.

Sagar, B. (1977). Downpull in High-head Gate Installations, Parts 1, 2, 3. *Water Power Dam Construct*, (3), 38–39; (4), 52–55; (5), 29–35.

Sagar, B. (2000). Gate Lip Hydraulics. *Water Power and Dam Construction*.